

We are IntechOpen, the world's leading publisher of Open Access books Built by scientists, for scientists

6,900

Open access books available

186,000

International authors and editors

200M

Downloads

Our authors are among the

154

Countries delivered to

TOP 1%

most cited scientists

12.2%

Contributors from top 500 universities



WEB OF SCIENCE™

Selection of our books indexed in the Book Citation Index
in Web of Science™ Core Collection (BKCI)

Interested in publishing with us?
Contact book.department@intechopen.com

Numbers displayed above are based on latest data collected.
For more information visit www.intechopen.com



Numerical Investigation of Heat Transfer and Fluid Flow Characteristics in a Rectangular Channel with Presence of Perforated Concave Rectangular Winglet Vortex Generators

Syaiful and M. Kurnia Lutfi

Abstract

The high thermal resistance of the airside of the compact heat exchanger results in a low heat transfer rate. Vortex generator (VG) is one of the effective passive methods to increase convection heat transfer by generating longitudinal vortex (LV), which results in an increase in fluid mixing. Therefore, this study aims to analyze the convection heat transfer characteristics and the pressure drop of airflow in a rectangular channel in the presence of a concave rectangular winglet VG on a heated plate. Numerical calculations were performed on rectangular winglet pairs vortex generators (RWP VGs) and concave rectangular winglet pairs vortex generators (CRWP VGs) with a 45° angle of attack and one, two, and three pairs of VGs with and without holes. The simulation results show that the decrease in the value of convection heat transfer coefficient and pressure drop on CRWP with three perforated VG configuration is 4.63% and 3.28%, respectively, of the three pairs of CRWP VG without holes at an airflow velocity of 2 m/s.

Keywords: heat transfer, pressure drop, vortex generators, vortex intensity, synergy angle

1. Introduction

A compact heat exchanger is a heat exchanger with a large area to volume ratio so that it has a high surface area of heat transfer to volume [1]. Compact heat exchangers are widely used in the air conditioning, refrigeration, chemical, petroleum, and automotive industries. Fin and tube heat exchanger is one type of compact heat exchanger that is often encountered. One example is the condenser in air conditioning, where air is used as a refrigerant cooling medium. However, the high thermal resistance on the airside results in a low heat transfer rate [2]. Therefore, to increase the heat transfer rate, the thermal resistance needs to be lowered by increasing the convection heat transfer coefficient [3].

The method of increasing the convection heat transfer coefficient has become an interesting thing to investigate [1]. In general, the method of increasing the convection heat transfer coefficient is divided into two, namely the active method and the passive method [4]. The active method is a method that uses external energy to increase the rate of convection heat transfer, for example, by electrostatic fields, fluid vibration, and flow pulsation [1, 5]. In contrast, the passive method is a method that does not use external energy to increase the convection heat transfer rate. Passive methods are more often used than active methods because they are simpler and more effective [6]. The increase in the convection heat transfer rate in the passive method is performed by adding an insert structure and surface modification, which results in the formation of swirl flow [4, 6].

Vortex generator (VG) is an insert that produces vortices due to the formation of swirl flow, which increases the heat transfer rate [7–9]. The vortex can be divided into two, namely the transverse vortex and the longitudinal vortex [9]. The transverse vortex has a vortex axis that is perpendicular to the main flow. Meanwhile, the longitudinal vortex has a vortex axis parallel to the main flow. Longitudinal vortices are more efficient in increasing convection heat transfer because they can improve thermal performance better than transverse vortices with the same pressure drop. Longitudinal vortex causes increased fluid mixing, boundary layer modification, and flow instability resulting in increased convection heat transfer coefficient [10].

Various studies regarding the use of VGs to improve convection heat transfer have been carried out. A. Datta et al. (2016) conducted a numerical investigation of heat transfer on a rectangular microchannel installed with VGs with angle position variations in two VGs with a Reynolds number range of 200–1100 [11]. The simulation results proved that the increase in heat transfer is directly proportional to the increase in the Reynolds number and the angle of attack of VG. Installation of angle of attack of 30° with Reynolds number 600 is the best combination. In addition, H. Y Li (2017) conducted an experimental and numerical study on the case of fluid flow in a pin-fin heat sink mounted with a delta winglet vortex generator (DW VGs) [12]. The study was conducted to determine the effect of Reynolds number, angle of attack of VGs, and height of VGs on convection heat transfer. The results show that the increase in the Reynolds number causes a decrease in thermal resistance resulting in an increase in the convection heat transfer coefficient. The results of these studies also indicate that the angle of attack of 30° is the best. Meanwhile, the optimum VGs height is $3/2 H$.

In 2017, H.E. Ahmed et al. conducted a heat transfer study on a triangular duct with a DWP VGs in three-dimensional modeling with nanofluid flow [13]. The simulation results showed an increase in heat transfer and pressure drop of 45.7% and $< 10\%$ respectively due to the installation of VGs and 3% Al_2O_3 nanoparticles. Overall, the use of VGs and nanofluids can improve heat transfer with lower pressure drops. In addition, Syaiful et al. (2017) conducted a numerical study of the installation of CDW VGs on rectangular channels [14]. The results showed that the increase in the heat transfer coefficient due to the installation of CDWP VGs is much better than DWP VGs. However, the use of CDWP VGs results in a higher increase in pressure drop. In general, the results showed that the increase in convection heat transfer coefficient and pressure drop due to the installation of three rows of CDW VGs are 42.2–110.7% and 180–266.9%, respectively.

Then, M. Oneissi et al. (2018) conducted a numerical study on the increase in heat transfer due to the installation of DWP VGs and inclined projected winglet pair VGs with the $k-\omega$ turbulent model [15]. In this three-dimensional simulation, the increase in heat transfer was viewed from the distribution of the Nusselt number, the coefficient of friction, and the vortices. The simulation results showed that the inclined projected winglet pair produces 7.1% better performance in increased heat

transfer than that of the DWP VGs. Zhimin Han et al. (2018) conducted a three-dimensional simulation study of the heat transfer characteristics through the perforated rectangular type of VGs [16]. In this study, the flow velocity was varied in the Reynolds number range of 214–10,703. The simulation results showed that giving holes to VGs can reduce pressure drop. The optimal thermo-hydraulic performance was observed for VGs with a hole diameter of 5 mm.

In addition, M. Samadifar et al. (2018) studied the effect of a new type of VG with variations in the angle of attack on the increase in heat transfer in the plate-fin heat exchanger in the triangular channel [17]. Six types of VGs were used in this numerical simulation, namely rectangular VG, rectangular trapezium VG, angular rectangular VG, wishbone VG, intended VG, and wavy VGs. M. Samadifar et al. performed a numerical simulation approach with turbulent $k-\omega$ SST modeling. The simulation results showed that rectangular VGs provide a better heat transfer increase than other VGs, with an increase of 7%. The simulation results also showed that the best VGs installation is VGs with an angle of attack of 45°. Jiyang Li et al. (2019) investigated the increase in heat transfer in finless flat-tube heat exchangers due to the installation of double triangle, triangular, and rectangular VG [18]. In modeling, VGs were installed in front of the finless heat exchanger with a distance of 1 mm so that the condensation water does not hit VGs. The results showed that VGs could disturb the thermal boundary layer so that the mixing of cold and hot air increases, which results in an increase in heat transfer performance. In addition, the results also showed that the double triangle VG increases the heat transfer coefficient by 92.3% at an air velocity of 2 m/s. The double triangle VGs increase the heat transfer coefficient by 20% greater than that of the triangular and rectangular VGs but also an increase in pressure drop.

G. Lu and X. Zhai (2019) conducted a numerical investigation of the flow characteristics through the curved VG on the fin and tube heat exchanger [19]. G. Lu and X. Zhai varied the curvature and angle of attack of VG in their research. Flow characteristics were reviewed based on several non-dimensional parameters, namely Nu/Nu_0 , f/f_0 and $R = (Nu/Nu_0)/(f/f_0)^{1/3}$ with a Reynolds number range of 405–4050. Their results showed that the best thermal-hydraulic performance was obtained for VG at a curvature of 0.25 with a value of $R = 1.06$ at a 15° angle of attack. R.K.B. Gallegos and R.N. Sharma (2019) also conducted heat transfer experiments due to the installation of VG flapping flags on the rectangular channel [20]. Their experimental results showed that VG increases the flow instability and the turbulence rate so that the Nusselt number increases by 1.34 to 1.62 times. However, VG also causes an increase in pressure drop because of the resistance to VG. This can be identified by an increase in the friction factor, which increased by 1.39–3.56 times.

The use of VG causes an increase in thermal performance, but its use has an impact on an increase in pressure drop, which results in low hydraulic flow performance. This study discusses the effect of installing RWP VGs and CRWP VGs on thermal and hydraulic performance. Thermal performance is investigated through analysis of the field synergy angle, spanwise average Nusselt number, and convection heat transfer coefficient values. Meanwhile, the hydraulic performance is analyzed through an increased pressure drop. This study aims to determine the effect of the type of VG and the effect of giving a hole on VG on thermal-hydraulic performance.

2. Physical model

2.1 Experimental set-up

Experiments on the effect of VG on heat transfer and pressure drop flow were carried out in a rectangular channel made of glass with a thickness of 1 cm and a

length of 370 cm, a width of 8 cm, and a height of 18 cm, as shown in **Figure 1**. The blower sucks air into the channel from the inlet side through a straightener composed of pipes with a diameter of 5 mm and wire mesh to equalize the flow velocity. The flow velocity in the channel was varied in the range of 0.4 m/s to 2.0 m/s with an interval of 0.2 m/s using a motor regulator controlled by an inverter (Mitsubishi Electric-type FR-D700 with an accuracy of ± 0.01 Hz) and measured with a hotwire anemometer (Lutron type AM-4204 with an accuracy of ± 0.05). In this study, the airflow flowed through VGs with variations in the number of rows (one, two, and three rows) as well as variations with/without holes to investigate the effect on heat transfer rate and pressure drop. The VGs were mounted on a flat plate that was heated at a constant rate of 35 W using a heater that was regulated by a heater regulator and monitored by a wattmeter (Lutron DW-6060 with an accuracy of ± 0.01). Thermocouples K type was used to measure surface temperature, inlet and outlet temperatures, which were connected to data acquisition (Advantech type USB-4718 with accuracy ± 0.01) and were monitored and stored in the CPU. In the pressure drop test, two pitot tubes were installed at the inlet and outlet of the test section and connected to a micro manometer (Fluke 922 with accuracy ± 0.01) to monitor the pressure drop due to the installation of VGs. Flow visualization tests were also carried out to observe the longitudinal vortex formed as a result of VGs insertion. The longitudinal vortex was formed when the smoke resulting from the evaporation of oil in the heater was flowed through VGs and captured by the transverse plane formed by the luminescence of the laser beam. The camera was used to record the longitudinal vortex structure that was formed.

2.2 Computational model

In this study, the effects of the installation of RWP and CRWP VGs in the rectangular channel on thermal–hydraulic performance were compared. The geometry of the VG used in this study can be seen in **Figure 2**. In this simulation, VGs were made from an aluminum plate with a thickness of 1 mm with/without holes

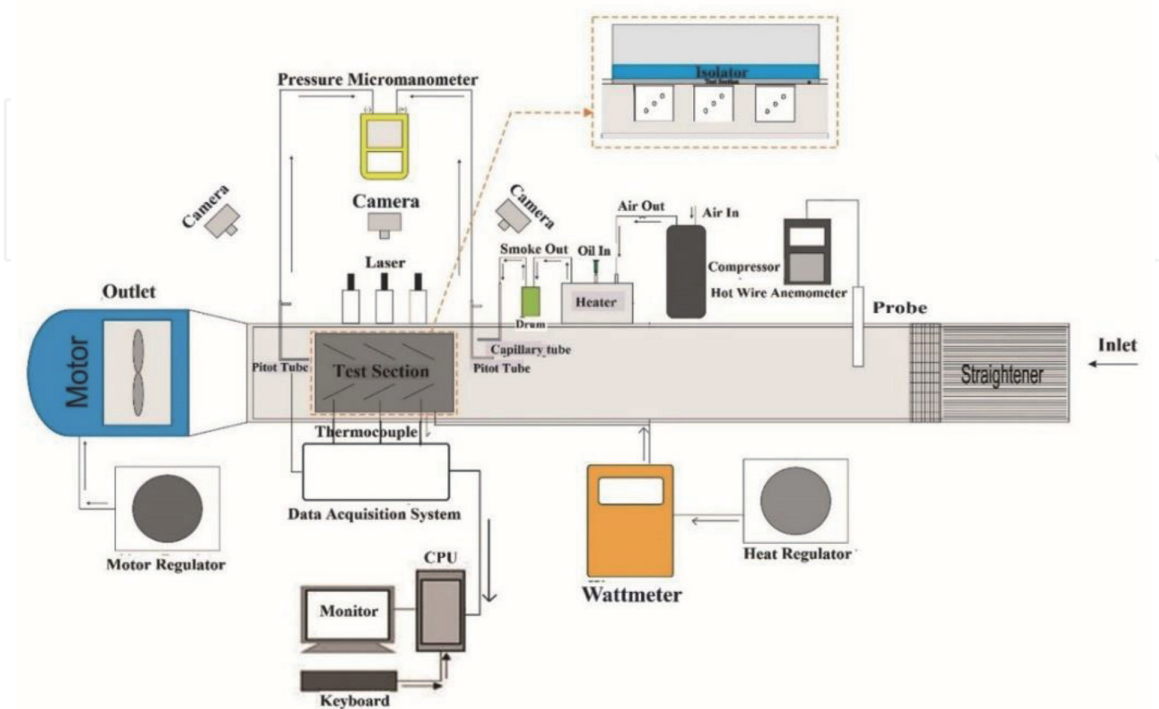


Figure 1.
Schematic of experimental set-up.

with a diameter of 5 mm. **Table 1** shows the geometric parameters of the CRWP and RWP VGs. **Figure 3** is a top view of the RWP and CRWP VGs. VG with the angle of attack (α) 45° arranged in-line in common flow-down orientation with a longitudinal pitch of 125 mm. The distance between the first row and the inlet channel is 125 mm. Meanwhile, the leading-edge transverse distance between winglet pairs VG is 20 mm. The rectangular channel modeled in this simulation has dimensions of length (P), width (L), height (H) of channels of 500 mm, 75.5 mm, 65 mm, respectively.

Figure 4 shows the computational domain used in this modeling. This domain consists of an inlet extended region and an outlet extended region. An inlet extended region was provided to ensure that the airflow entering the channel is a fully developed flow. Meanwhile, an extended region outlet was added so that the air does not experience reverse flow in the channel.

2.3 Governing equations

In this 3-D flow modeling, air was assumed to be steady state, incompressible and has constant physical properties. Flow can be laminar or turbulent based on its

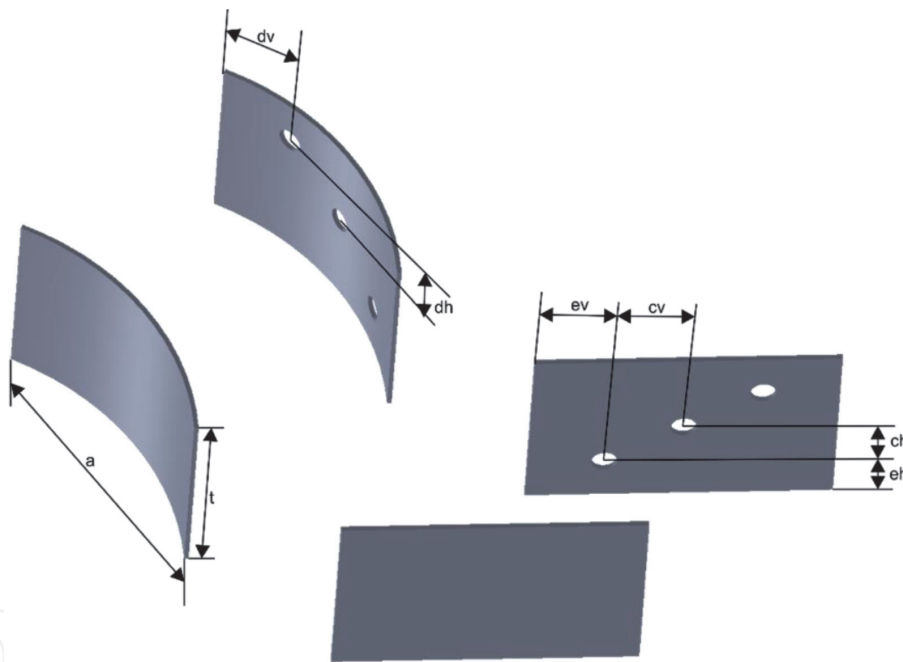


Figure 2.
 Geometry of RWP and CRWP VG with and without holes.

VGs	α ($^\circ$)	a (mm)	cv (mm)	dv (mm)	ev (mm)	ch (mm)	dh (mm)	eh (mm)	t (mm)	R (mm)
CRWP without holes	45	59	—	—	—	—	—	—	40	58
CRWP with holes	45	59	15	14.56	—	—	20	9.85	40	58
RWP without holes	45	60	—	—	—	—	—	—	40	—
RWP with holes	45	60	15	—	15	20	—	10	40	—

Table 1.
 Geometry parameters of vortex generator (VG).

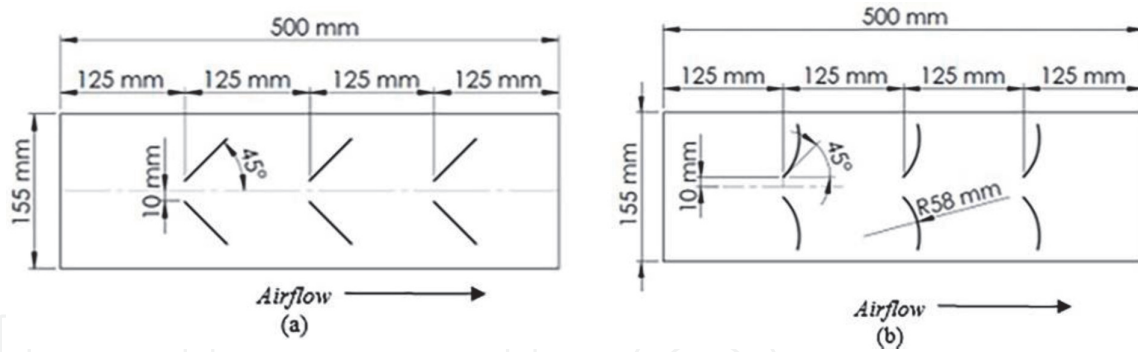


Figure 3.
Top view of (a) RWP VG, (b) CRWP VG.

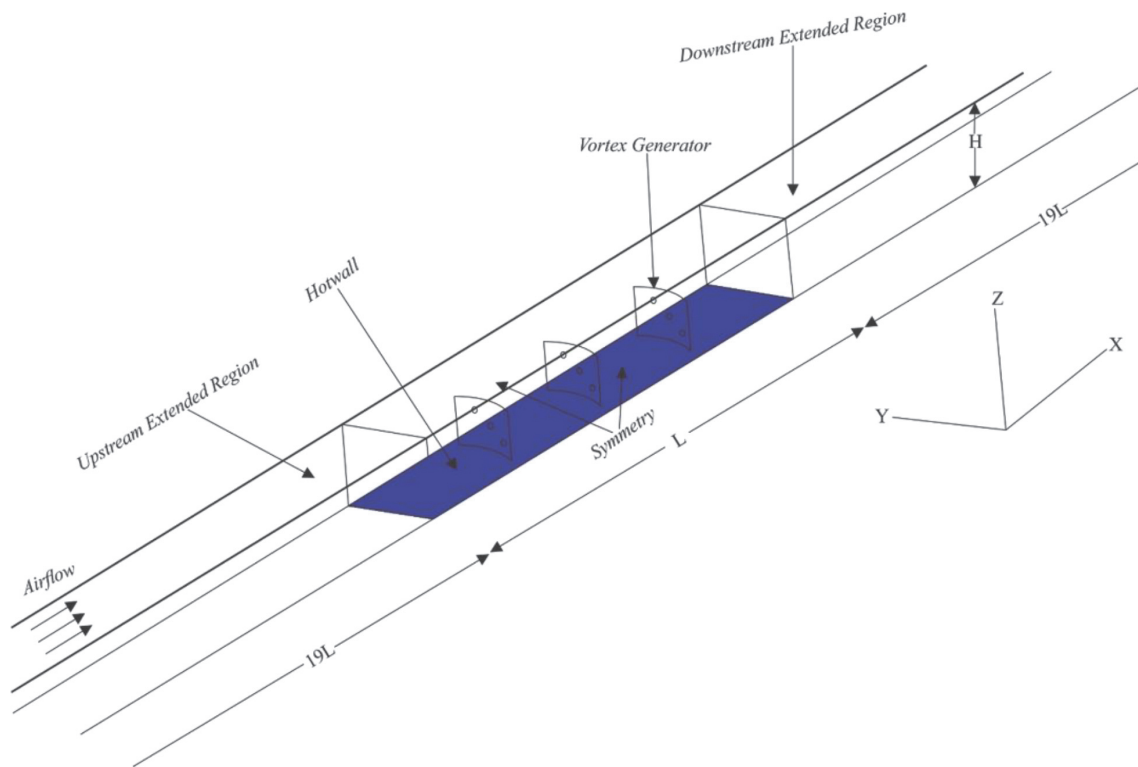


Figure 4.
Computational domain.

Reynolds number value. Flow velocities were set in the range of 0.4–2 m/s with 0.2 m/s intervals. The Reynolds number is determined from $\mathfrak{R} = \rho u_m D_h / \mu$ in the range of $1800 < \text{Re} < 9100$. Therefore, the flow was assumed to be laminar at a velocity of 0.4 m/s with $\text{Re} = 1800$ and the others were turbulent. Based on these assumptions, the governing equations used to solve this case are:

Continuity equation

$$\frac{\partial u_j}{\partial x_j} = 0 \quad (1)$$

Momentum equation

$$\frac{\partial}{\partial x_j} (\rho u_i u_j) = -\frac{\partial p}{\partial x_i} + \frac{\partial}{\partial x_j} \left(\mu \frac{\partial u_k}{\partial x_i} \right) \quad (2)$$

Energy equation

$$\frac{\partial}{\partial x_i} (\rho u_i T) = \frac{\partial}{\partial x_i} \left(\Gamma \frac{\partial T}{\partial x_i} \right) \quad (3)$$

where ρ , p , u_i , and μ are the density, pressure, mean velocity on the x-axis, and dynamic viscosity, respectively. Meanwhile, Γ is the diffusion coefficient

$$\Gamma = \lambda / c_p$$

where λ is the thermal conductivity, and c_p is the specific heat of air.

The turbulent flow modeling used in this simulation is the standard k - ω model. The transport equation for the standard k - ω model consists of the turbulent kinetic energy (k) and specific dissipation rate (ω) equations, respectively, which are stated as follows:

$$\frac{\partial}{\partial x_i} (\rho k u_i) = \frac{\partial}{\partial x_j} \left(\Gamma_k \frac{\partial k}{\partial x_j} \right) + G_k - Y_k + S_k \quad (4)$$

$$\frac{\partial}{\partial x_i} (\rho \omega u_i) = \frac{\partial}{\partial x_j} \left(\Gamma_\omega \frac{\partial \omega}{\partial x_j} \right) + G_\omega - Y_\omega + S_\omega \quad (5)$$

where Γ_ω is the specific dissipation rate and Γ_k is the diffusion effectiveness of turbulence kinetic energy. The Γ_ω and Γ_k equations are stated as follows:

$$\Gamma_\omega = \mu + \frac{\mu_t}{\sigma_\omega} \quad (6)$$

$$\Gamma_k = \mu + \frac{\mu_t}{\sigma_k} \quad (7)$$

σ and μ_t are the turbulent Prandtl number and turbulent viscosity, respectively. In this governing equation, the turbulent intensity can be formulated as follows:

$$I = 0.16 \mathcal{R}_{D_h}^{-1/8} \quad (8)$$

2.4 Boundary conditions

The boundary conditions used in this computational domain are described as follows:

Inlet upstream extended region

$$u = u, v = w = 0, T = T = Const. \quad (9)$$

Outlet downstream extended region

$$\frac{\partial u}{\partial x} = \frac{\partial v}{\partial x} = \frac{\partial w}{\partial x} = \frac{\partial T}{\partial x} = 0 \quad (10)$$

Wall

$$u = v = w = 0, T = T_w \quad (11)$$

Symmetry

$$v = 0, \frac{\partial u}{\partial y} = \frac{\partial w}{\partial y} = \frac{\partial T}{\partial y} = 0 \quad (12)$$

2.5 Numerical method

The finite volume method (FVM) was used to analyze the thermo-hydraulic characteristics of the rectangular channel installed with VGs. Laminar flow was simulated using a laminar model, while the turbulent flow was simulated using the $k-\omega$ model. The turbulent $k-\omega$ model was used in this simulation because this model is suitable for modeling fluid flow in the viscous region [21]. The SIMPLE algorithm was chosen to obtain a numerical solution of the continuity and momentum equations. The governing equations for momentum, turbulent kinetic energy, specific dissipation rate and energy were discretized with a second-order upwind scheme. The convergence criterion assigned to the continuity, momentum, and energy equations was 10^{-5} , 10^{-6} , 10^{-8} , respectively.

In this numerical simulation, the mesh type was differentiated between the upstream extended and downstream extended regions with the computational domain, as shown in **Figure 5**. The hexagonal mesh was used in both parts of the extended region because it has a simple geometric shape. Meanwhile, the part of the computational domain, namely the fluid and plate, uses a tetrahedral mesh because it has a more complex geometry due to the presence of VGs. The tetrahedral mesh was also used to obtain more accurate results in this area so that it can show flow separation and secondary flow in the test section.

2.6 Parameter definitions

The parameters used in this study are as follows:

Reynolds number

$$\Re = \frac{\rho u_m D_h}{\mu} \quad (13)$$

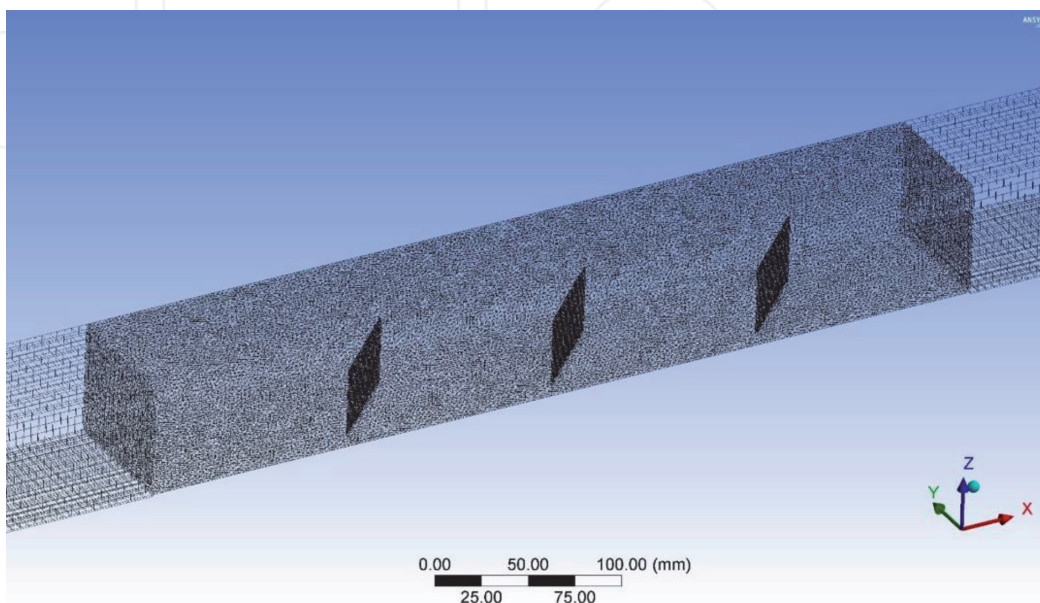


Figure 5.
Mesh generated.

Nusselt number

$$Nu = \frac{hD_h}{\lambda} \quad (14)$$

where ρ , u_m , μ , D_h , and λ are the density, average fluid velocity, dynamic viscosity, hydraulic diameter, and thermal conductivity of the fluid, respectively. h is the convection heat transfer coefficient obtained from the following equation:

$$h = \frac{q}{A_T(T_w - T_f)} \quad (15)$$

q , A_T , and T_w are the convection heat transfer rate, heat transfer surface area, and hot wall temperature, respectively, while T_f is the bulk fluid temperature which is defined as follows:

$$T_f = \frac{T + T_{out}}{2} \quad (16)$$

T_{in} is the inlet temperature and T_{out} is the temperature at the outlet side which is determined by the following equation:

$$T = \frac{\iint_A u(x, y, z)T(x, y, z)dA}{\iint_A u(x, y, z)dA} \quad (17)$$

$$T_{out} = \frac{\iint_{A_{out}} u(x, y, z)T(x, y, z)dA}{\iint_{A_{out}} u(x, y, z)dA} \quad (18)$$

ΔP is the pressure drop of fluid flow which can be formulated as $\Delta P = P_{in} - P_{out}$ in which P_{in} and P_{out} can be described as follows:

$$P = \frac{\iint_A p dA}{\iint_A dA} \quad (19)$$

$$P_{out} = \frac{\iint_{A_{out}} p dA}{\iint_{A_{out}} dA} \quad (20)$$

2.7 Validation

An independent grid test was performed to ensure that the number of grids does not affect the numerical simulation results. Four different grid numbers were used for grid-independent testing. The test was carried out on the computational domain with three CRWP pairs at a velocity of 0.4 m/s. **Table 2** shows the simulation results of the variation in the number of different grids on the convection heat transfer coefficient. Because the convection heat transfer coefficient of the simulation results shows a slight difference, the optimum number of grids is determined by comparing the heat transfer coefficient from the modeling results and the results from the experiment. The smallest error from the simulation results and experimental results is used as an independent grid. Based on the comparison of the simulation results for the various numbers of grids with the experimental results, it is found that the grid with the number of elements close to 1,600,000 was chosen for use in this numerical simulation because it has the lowest error, namely 0.337%. Validation was also carried out by comparing the

Number of element	h(simulation)	h(experiment)	Error (%)
1,262,840	18.27726	18.18571	0.503
1,478,060	18.34781	18.18571	0.891
1,661,610	18.24699	18.18571	0.337
1,868,587	18.29429	18.18571	0.597

Table 2.
Grid independent test.

experimental results of Wu et al. (2008) and current experimental results with slightly different conditions, see Ref. [22].

3. Results and discussion

This study aims to investigate the effect of holes on VGs and the number of pairs of VGs on airflow and heat transfer characteristics. The installation of VG generates vortices and forms swirl flow so that the convection heat transfer rate on the airside increases [7–9].

3.1 Flow field

To determine the difference in flow structure in the test section, simulations were carried out on a channel with VGs and without VGs (baseline). **Figure 6(a)** is a flow in the baseline case where vortices and swirl flows are not observed. Whereas in **Figure 6(b)**, the simulation results show that the installation of VGs on the channel results in the formation of swirl flow [7], which results in longitudinal vortices due to flow separation along the VGs caused by pressure differences on the upstream and downstream VGs [10]. **Figure 7** illustrates the counter-rotating pairs of longitudinal vortices due to the installation of RWPs and CRWPs VGs with a 45° angle of attack. A strong counter-rotating longitudinal vortex forms behind the VG with the left rotating clockwise and the right rotating counterclockwise [23]. These two longitudinal vortices result in the formation of downwash flow in the center of the channel towards the lower wall of the channel and upwash flow on both sides of the channel to the upper wall of the channel. This longitudinal vortex configuration is also called common-flow-down.

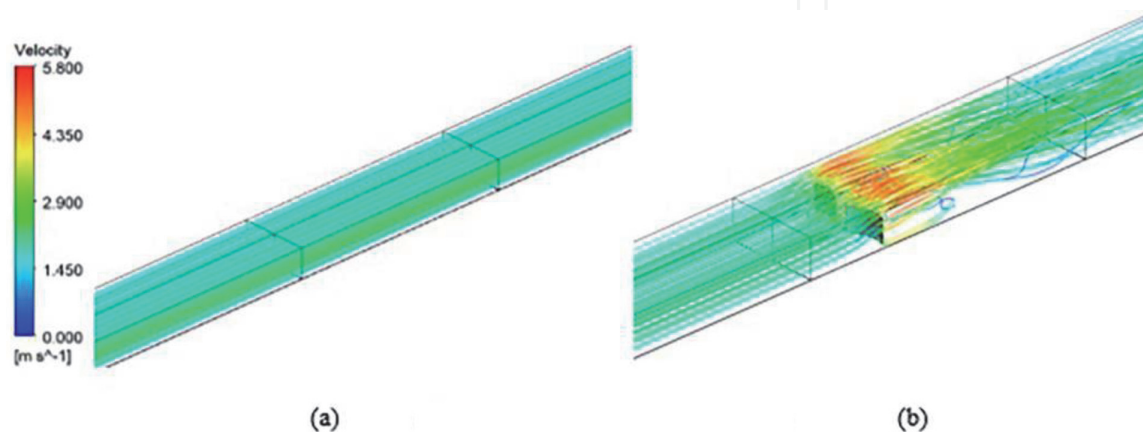


Figure 6.
Velocity streamline in a channel; (a) without VG (baseline), (b) with VG.

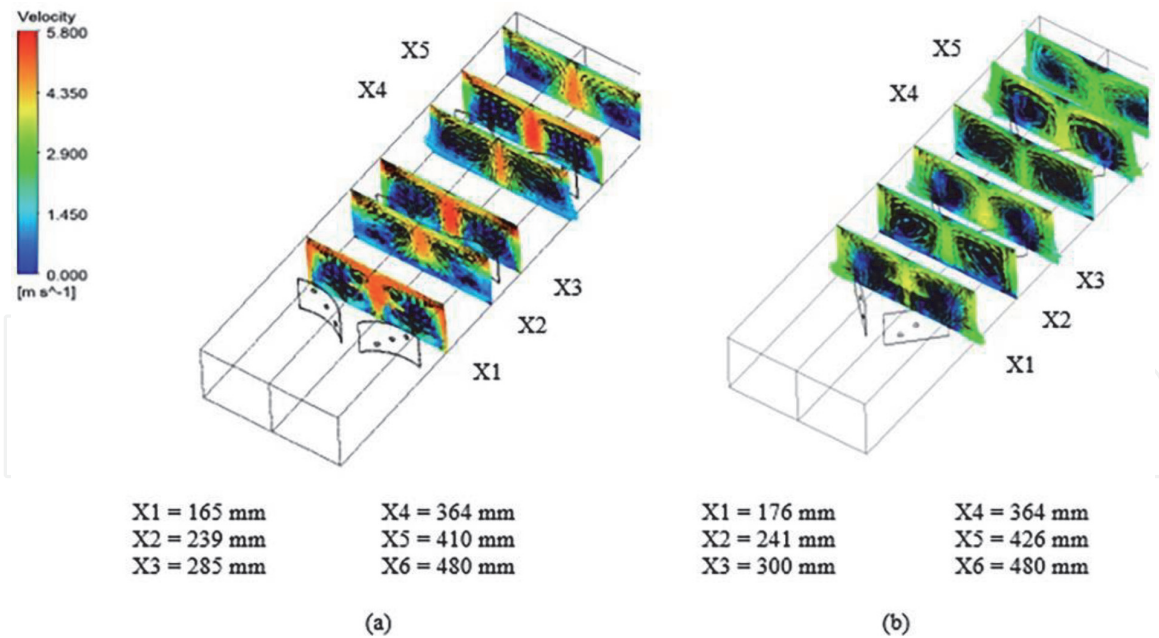


Figure 7.
 Tangential velocity vector on a channel with three pairs of VG: (a) perforated CRWP and (b) perforated RWP.

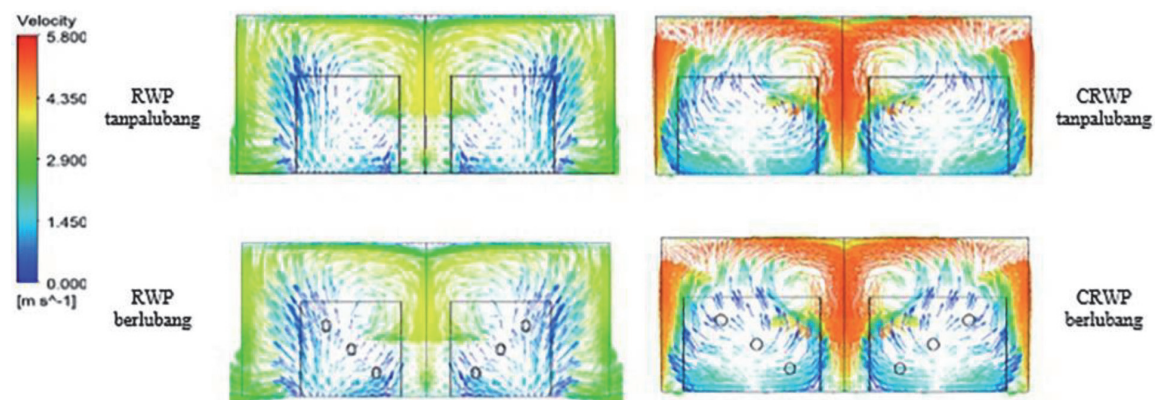


Figure 8.
 Tangential velocity vector in the cross-section X1.

Figure 8 is a comparison of tangential velocity vectors in the cross-plane X1 with three pairs of RWP and CRWP VGs for with and without holes at 2.0 m/s. The tangential velocity vector in the use of RWP and CRWP VGs is high in the down-wash region, which results in improved heat transfer [7]. In the case of CRWP VGs, the longitudinal vortex radius formed is larger than that of the RWP VGs. This is because the frontal area of the CRWP is larger, which results in a better heat transfer rate increase than that of the RWP VGs [24, 25]. The hole in VG causes a jet flow, which removes stagnant fluid in the back region of VG and increases the kinetic energy in this area so that the pressure difference before and after passing VG can be reduced [26]. Because of this decrease in the pressure difference, the longitudinal vortex strength decreases. The main vortex, induced vortex, and corner vortex are observed on CRWP VGs installation, as shown in **Figure 9**. The structure of the longitudinal vortex is formed due to several factors. The main vortex is formed due to flow separation when the flow passes through the VG wall due to the pressure difference [27]. Induced vortex is formed due to the interaction between the main vortex. Meanwhile, the corner vortex is formed as a result of the interaction between the VG wall and the main vortex.

Figures 10 and 11 show the counter-rotating longitudinal vortex as the flow passes through the VGs. Counter-rotating longitudinal vortices are observed in the

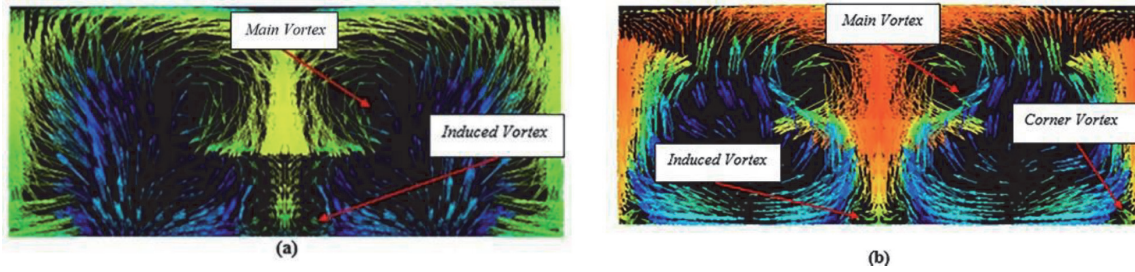


Figure 9. Tangential velocity vector in the cross-section X_1 in the channel installed VG: (a) perforated RWP, (b) perforated CRWP.

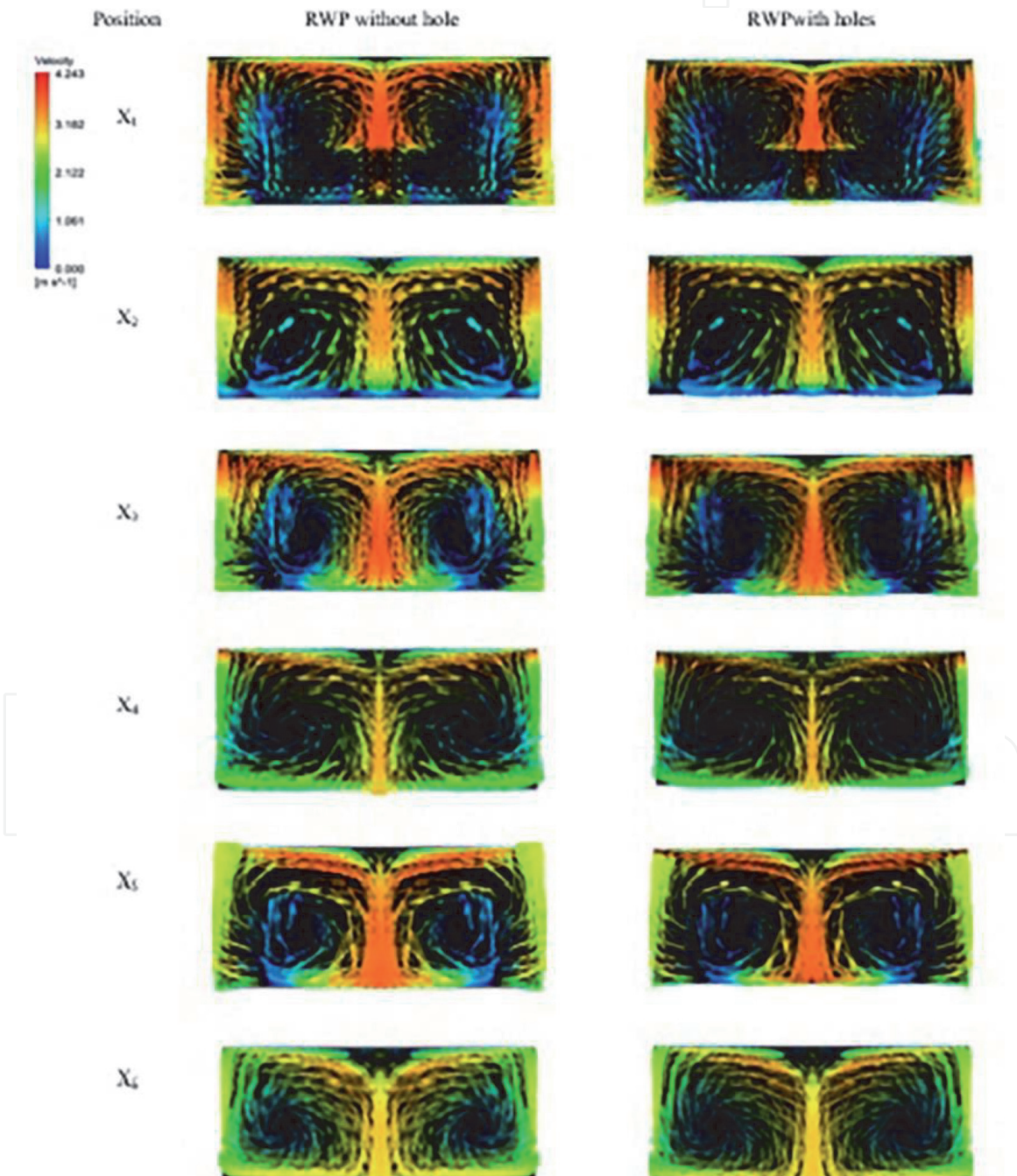


Figure 10. Comparison of the tangential velocity distribution in the channel installed RWP at several cross-section positions at a velocity of 2.0 m/sec.

cross-sectional plane at positions X1 to X6 and move spirally downstream to a certain distance and sweep towards the lower wall of the channel [26]. The strength of the longitudinal vortex is observed to be greater in CRWP than in RWP. CRWP has greater longitudinal vortex strength because CRWP has a larger frontal area than that of RWP, which results in a larger longitudinal vortex radius causing in better heat transfer performance [19]. From **Figures 10** and **11**, it is observed that the longitudinal vortex in the X1 plane is stronger than that in the X2 plane for all types of VG with/without holes. This is due to viscous dissipation, which causes the longitudinal vortex to gradually weaken as the flow away from VG [28]. In the X3 plane, the longitudinal vortex strength increases compared to the X2 plane due to the addition of VGs, which results in an increase in fluid velocity in the downwash region [29]. The hole in the VG results in the weakening of the longitudinal vortex strength due to jet flow formation [26].

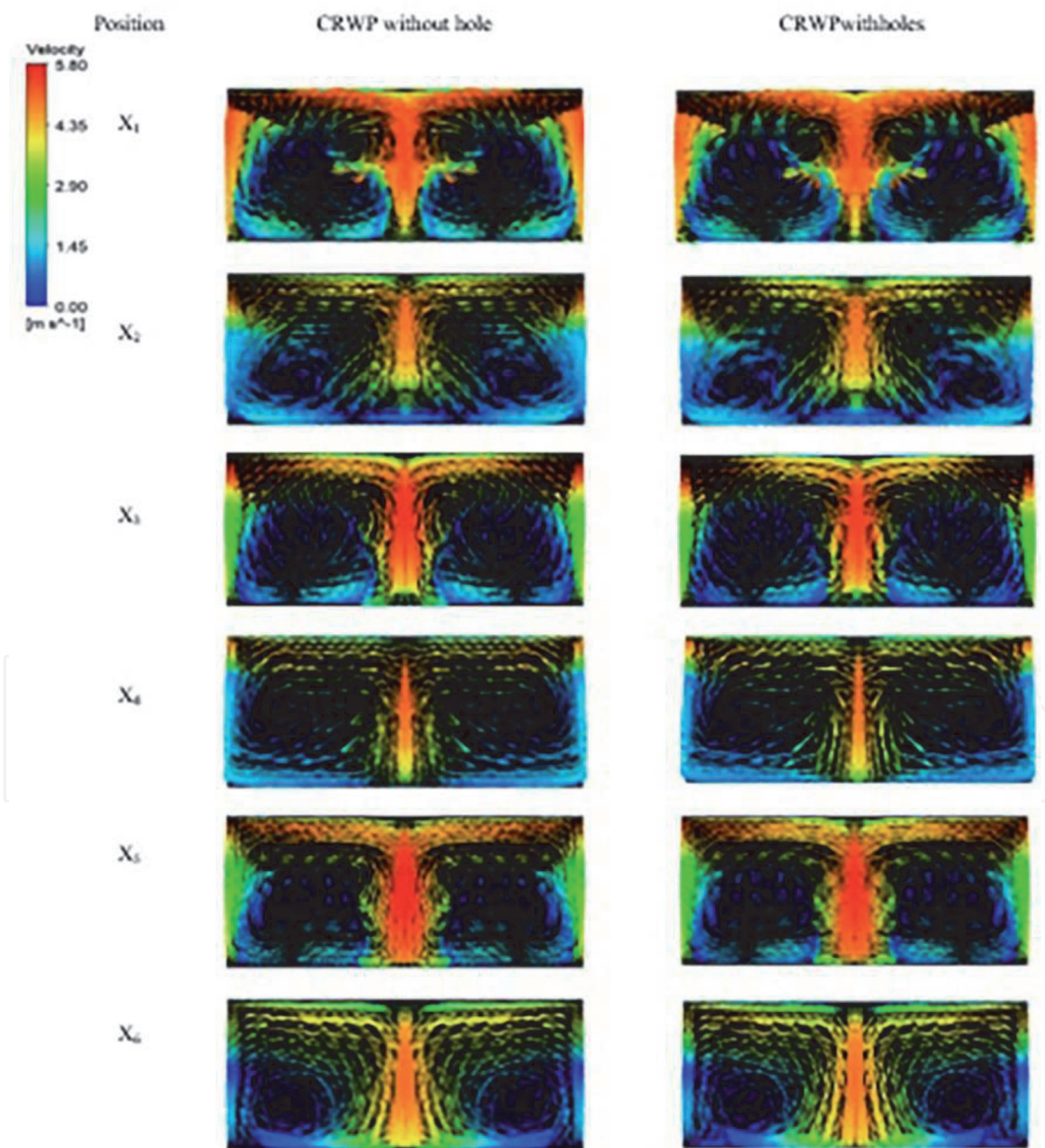


Figure 11. Comparison of the tangential velocity distribution in the channel installed CRWP at several cross-section positions at a velocity of 2.0 m/sec.

3.2 Longitudinal vortex intensity

The longitudinal vortex intensity is a dimensionless number studied by K Song et al. [30] and represents the magnitude of the inertia force induced by secondary flow to the viscous force. In this study, the longitudinal vortex intensity is defined in Eq. (22)

$$Se = \frac{\rho D_h U}{\mu} \quad (21)$$

where Se is the longitudinal vortex intensity, and U is the secondary flow velocity characteristic, which can be formulated in the following equation:

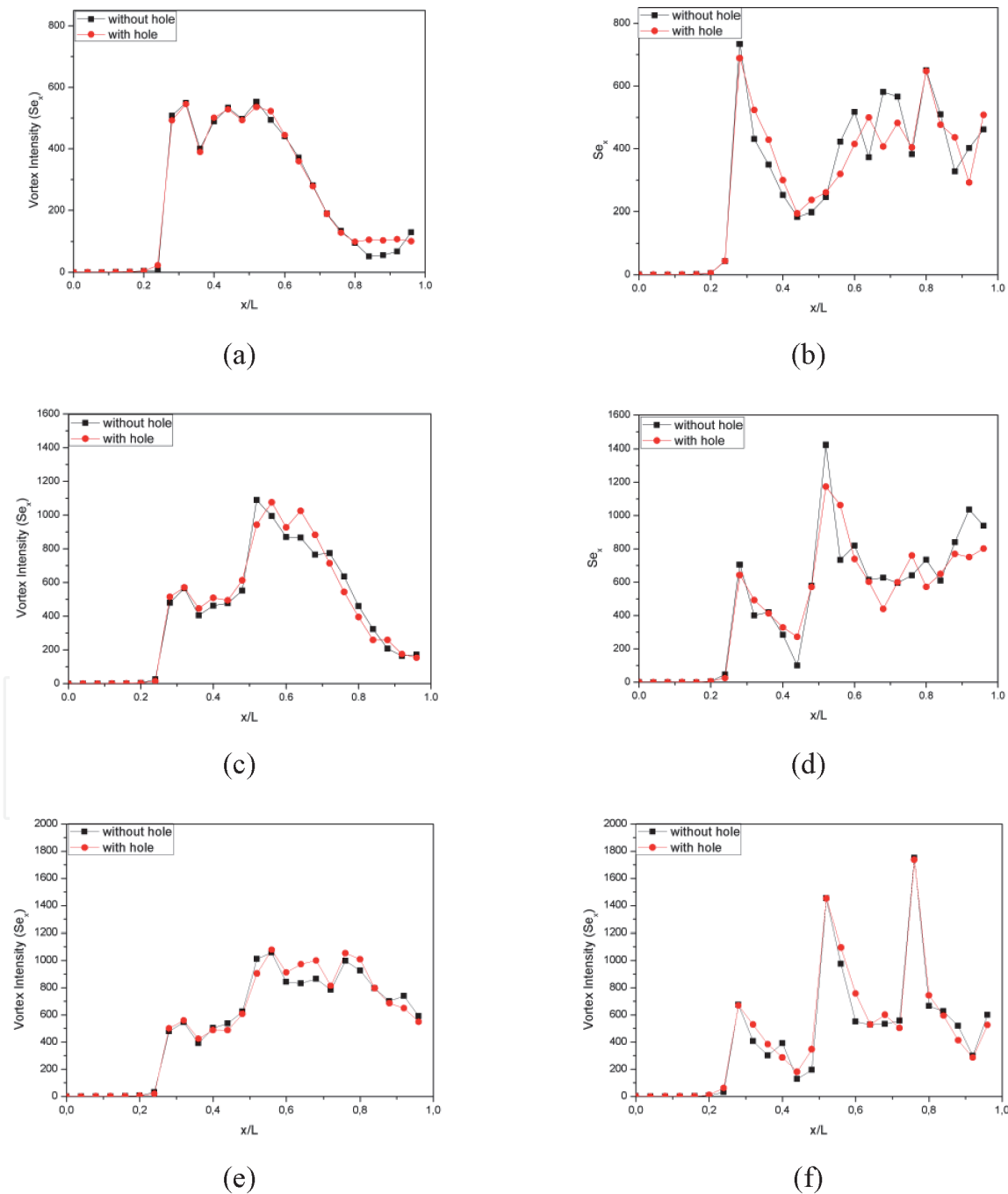


Figure 12. The mean spanwise longitudinal vortex intensity at a velocity of 0.4 m/s for the case of (a) one-pair RWP; (b) one-pair of CRWP; (c) two pairs RWP; (d) two-pairs CRWP; (e) three pairs RWP; (f) three-pairs CRWP.

$$U = D_h |\omega^n| = D_h \left| \frac{\partial w}{\partial y} - \frac{\partial v}{\partial z} \right| \quad (22)$$

where ω^n is the vortices about the normal axis of the spanwise plane. The mean longitudinal vortex intensity in the spanwise plane at position x (Se_x) is defined by Eq. (24)

$$Se_x = \frac{\rho D_h^2}{A(x)\mu} \iint_{A(x)} |\omega^n| dA \quad (23)$$

Figures 12 and 13 show the ratio of Se_x in RWP and CRWP cases at a velocity of 0.4 m/s and 2.0 m/s. In general, CRWP insertion produces a greater longitudinal

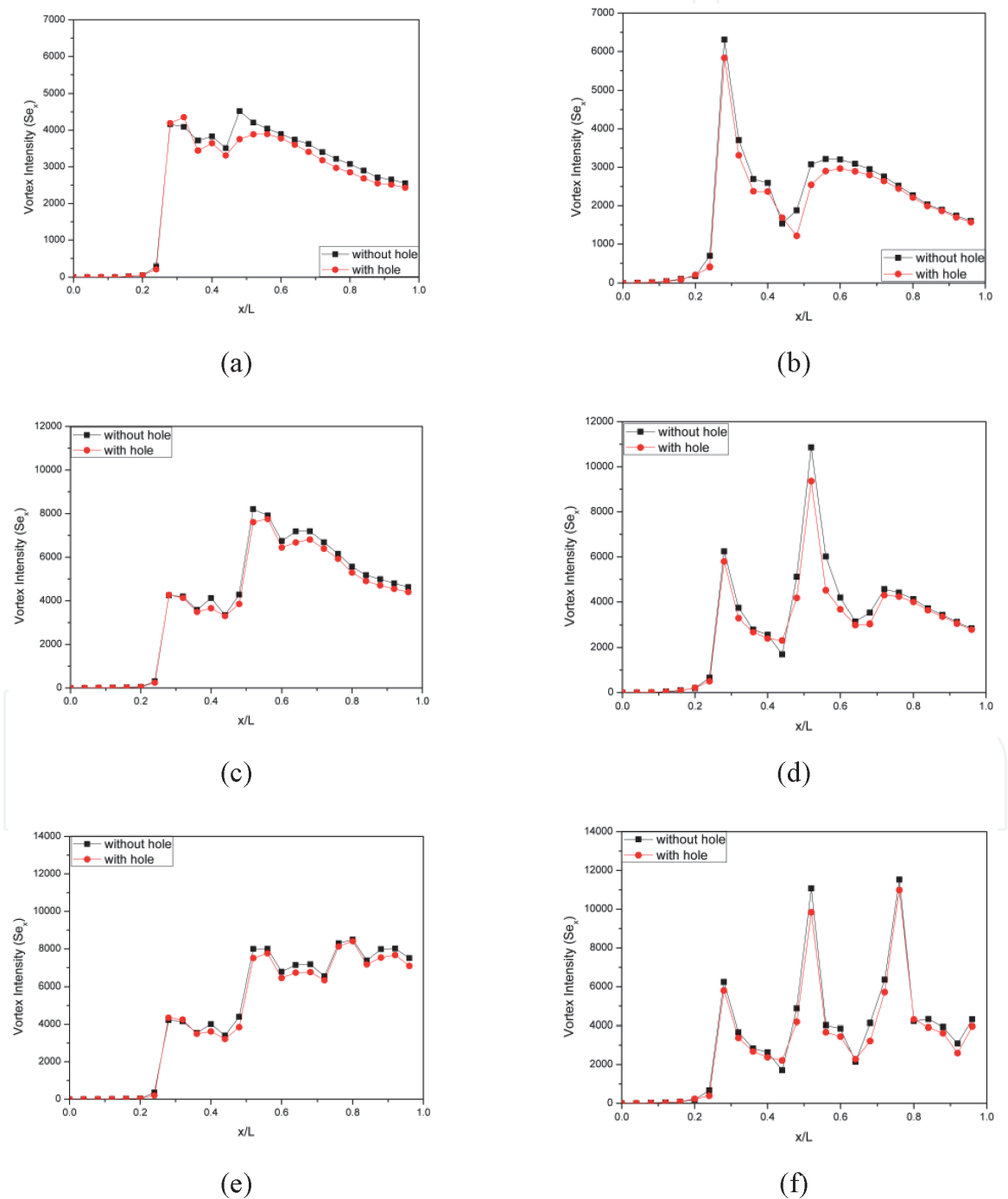


Figure 13. The mean spanwise longitudinal vortex intensity at a velocity of 2.0 m/s for the case of (a) one-pair RWP; (b) one-pair of CRWP; (c) two pairs RWP; (d) two-pairs CRWP; (e) three pairs RWP; (f) three-pairs CRWP.

vortex intensity than that of RWP because the frontal area of the CRWP is larger than that of the RWP and due to the instability of centrifugal force when the flow passes over the CRWP surface [19, 31]. The longitudinal distribution of the vortex intensity is shown in **Figure 14** for a velocity of 0.4 m/s and **Figure 15** for a velocity of 2.0 m/s. In the case of CRWP and RWP, the longitudinal vortex intensity tends to dissipate after passing VGs due to viscous effects [2, 26, 28]. Therefore, the installation of the second and third rows of VG reinforces the intensity of the longitudinal vortex as illustrated in **Figures 12(c)–(f)** and **Figures 13(c)–(f)** for velocities of 0.4 m/s and 2 m/s, respectively.

The hole in the VG results in a decrease in the intensity of the longitudinal vortex, as shown in **Figures 12–15**. The hole in VG causes jet flow formation, which can interfere with the generation of the longitudinal vortex [26]. For RWP VGs with a velocity of 2.0 m/s, the intensity of the longitudinal vortex experiences the highest decrease, namely 17% at $x/L = 0.48$ for the case of one pair with holes, 11% at $x/L = 0.4$ for the case of two pairs with holes and 13% at $x/L = 0.48$ for the case of three pairs with holes of ones without holes. Meanwhile, in the case of CRWP VGs with a velocity of 2.0 m/s, the intensity of the longitudinal vortex experiences the highest decrease, namely 35% at $x/L = 0.48$ for the case of one pair with holes, 14% at $x/L = 0.68$ for the case of two pairs with holes and 22% at $x/L = 0.68$ for the case of three pairs with holes compared to ones without holes.

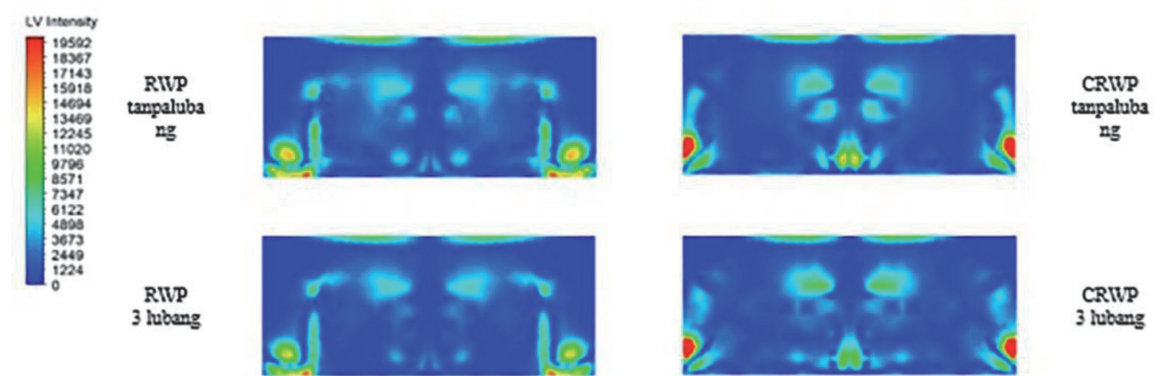


Figure 14. The longitudinal vortex intensity for the case of three pairs of RWP and CRWP at locations $x/L = 0.34$ and $x/L = 0.32$ at a velocity of 0.4 m/s, respectively.

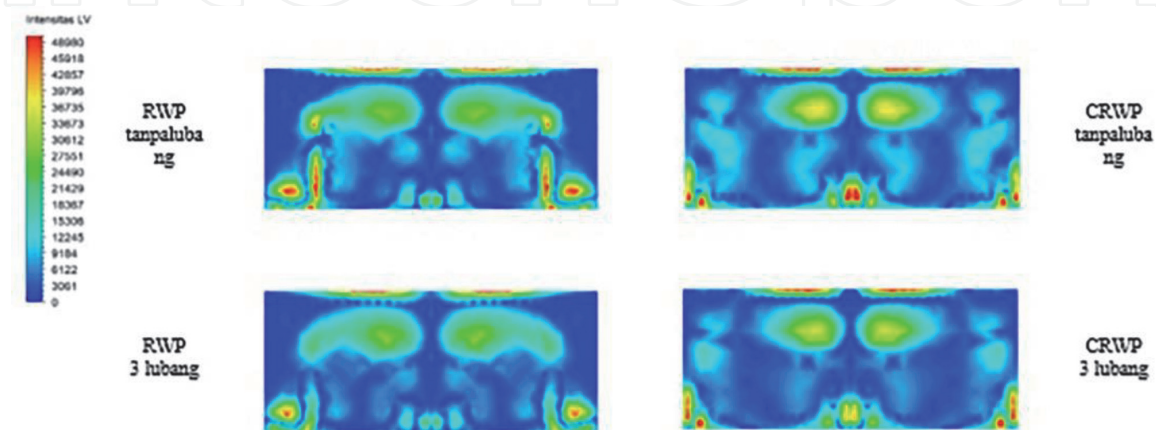


Figure 15. The longitudinal vortex intensity for the case of three pairs of RWP and CRWP at locations $x/L = 0.34$ and $x/L = 0.32$ at a velocity of 2.0 m/s, respectively.

3.3 Temperature distribution

The temperature distribution for the RWP and CRWP cases with/without holes and the baseline in the spanwise plane at a certain position with a velocity of 2.0 m/s is shown in **Figures 16** and **17**. Visually, the temperature distribution in the channel in the presence of VG is better than the baseline. The placement of VG in the channel increases the temperature distribution due to the counter-rotating pairs of longitudinal vortices, which result in increased fluid mixing [32]. Counter-rotating pairs of longitudinal vortices produce a downwash that pushes the fluid towards the surface of the heated plate resulting in increased local heat transfer coefficients and thinning of the thickness of the thermal and dynamic boundary layers [32, 33].

Meanwhile, counter-rotating pairs of longitudinal vortices also generate upwash on the outer side of the vortex and push the hot fluid on the plate wall towards the flow-stream resulting in a decrease in the local heat transfer coefficient and a

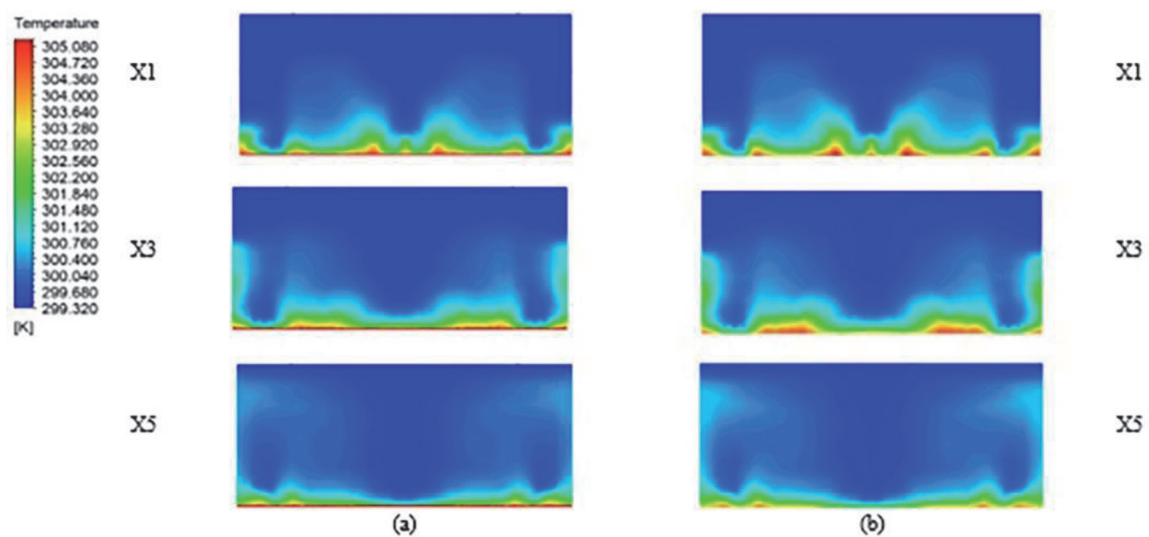


Figure 16.
 Temperature distribution in channel with: (a) RWP without holes; (b) RWP with holes.

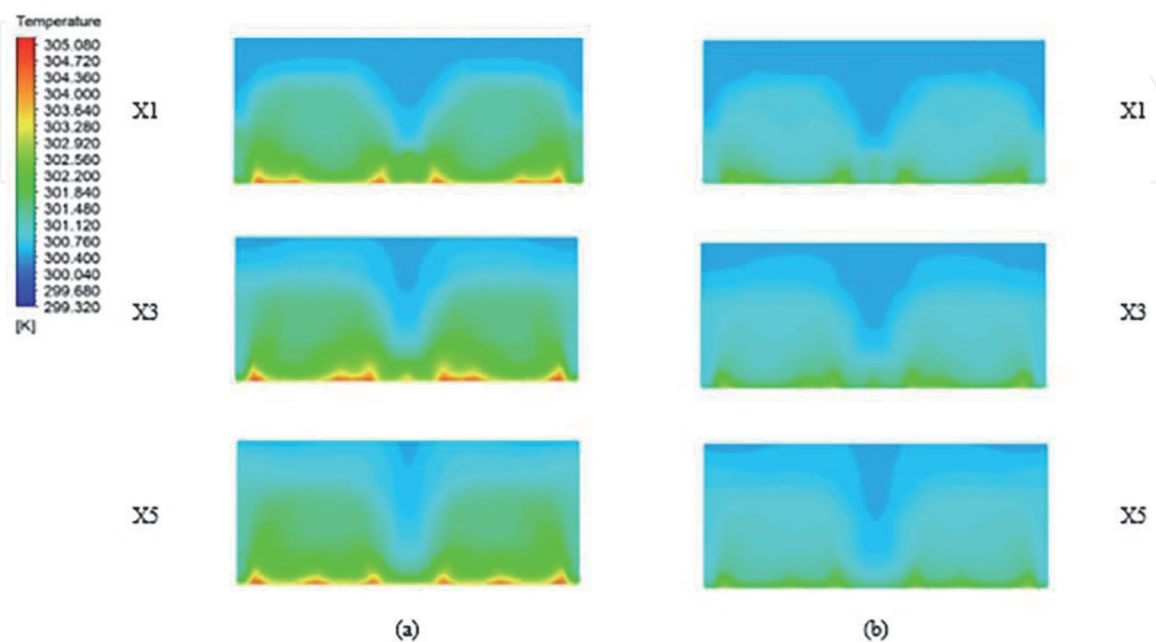


Figure 17.
 Temperature distribution in channel with: (a) CRWP without holes; (b) CRWP with holes.

thickening of the boundary layer as observed in **Figures 16** and **17** comparing to the baseline case, as shown in **Figure 18**. Visually, the temperature distribution in the CRWP case is more even than the temperature distribution in the RWP case. This is because CRWP produces a higher longitudinal vortex intensity than that of RWP [31]. In addition, the holes in each VG result in the formation of jet flow, which can reduce the intensity of the longitudinal vortex resulting in an increase in temperature gradient [26], as shown in **Figure 16(b)** and **17(b)**.

3.4 Pressure distribution

Figure 19 shows the pressure distribution for the three-pairs RWP and CRWP cases with/without holes at a Velocity of 2.0 m/s. Installation of VG in the channel results in an increase in pressure drop due to drag generated on the flow [34, 35]. As observed in Figure 3.14, the pressure drop generated by CRWP is higher than that from RWP. This is because the frontal area of the CRWP is larger than that of the RWP, which results in a higher longitudinal vortex intensity and results in increased pressure drop [19]. A low-pressure zone is formed behind VG in the RWP and CRWP cases [26]. The hole in VG causes in the formation of jet flow, which results in a decrease in the low-pressure zone. This is because the jet flow reduces the stagnant fluid in the area behind VG and increases the kinetic energy in this area, causing the pressure difference before and after passing VG to decrease [26].

3.5 Mean spanwise Nusselt number

The local heat transfer improvement can be identified with the mean spanwise Nusselt number, as informed by Hiravennavar [36]. The equation used by Hiravennavar is as follows:

$$\dot{N}u_s = \frac{Bq(H/k)}{\int_0^B (T_w - T_b) dz} \quad (24)$$

where B , q , H , and k are channel width, heat flux, channel height, and fluid thermal conductivity, respectively. Meanwhile, T_w and T_b are the wall temperature and bulk fluid temperature, respectively.

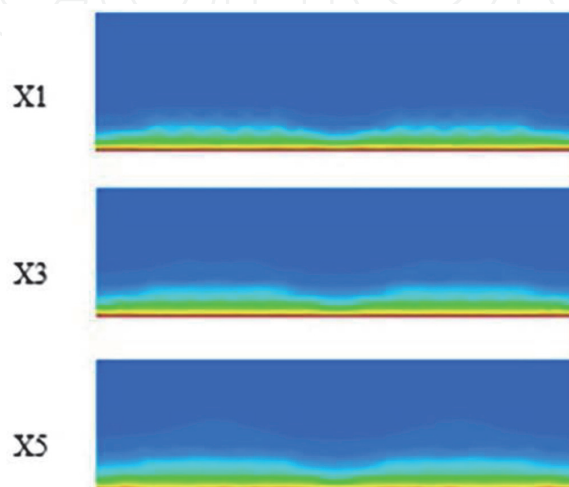


Figure 18.
Temperature distribution in the channel without VG (baseline).

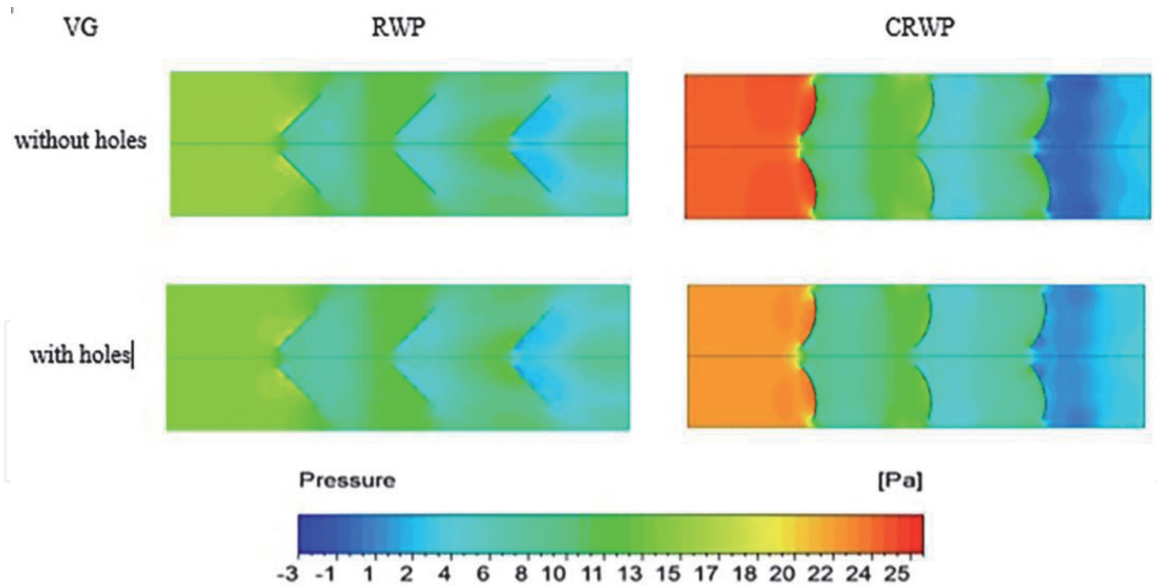


Figure 19.
 Comparison of the pressure distribution at $z = 0.41H$.

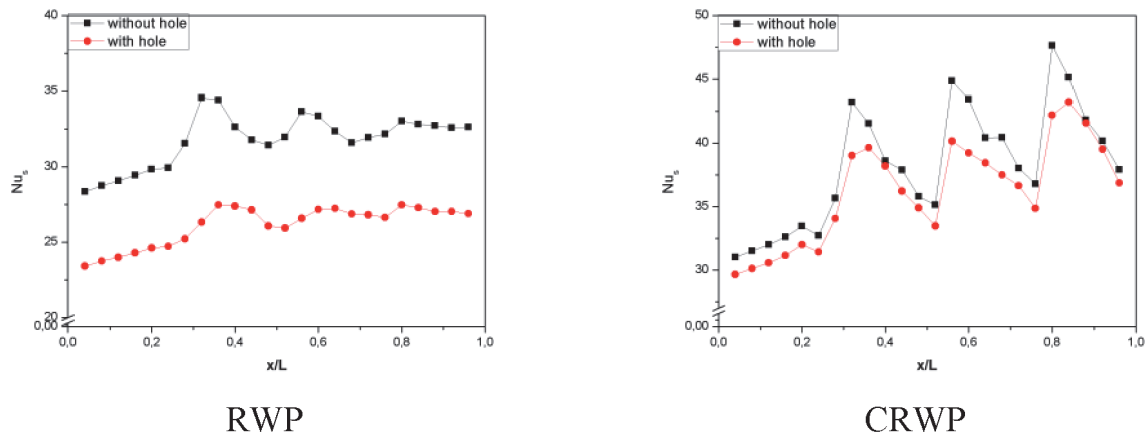


Figure 20.
 Average spanwise Nusselt numbers the RWP and CRWP at a velocity of 0.4 m/s.

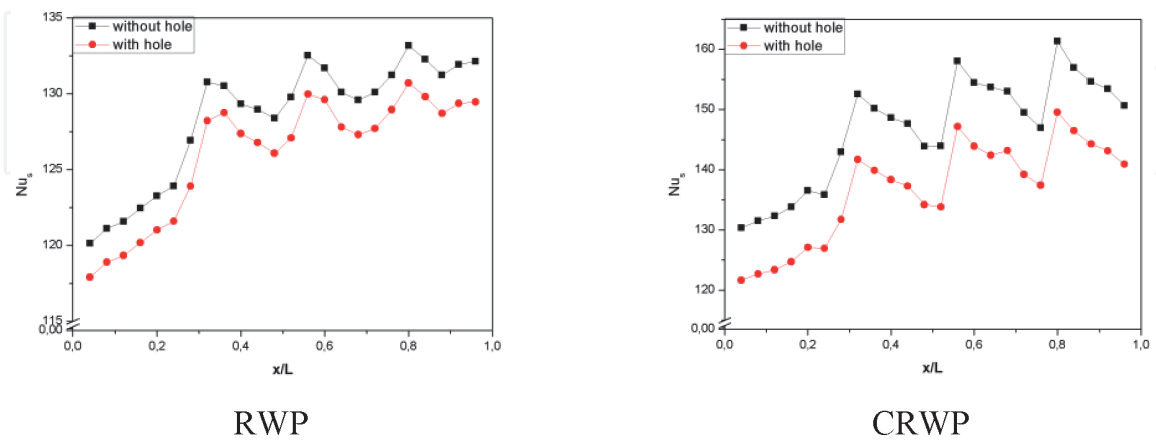
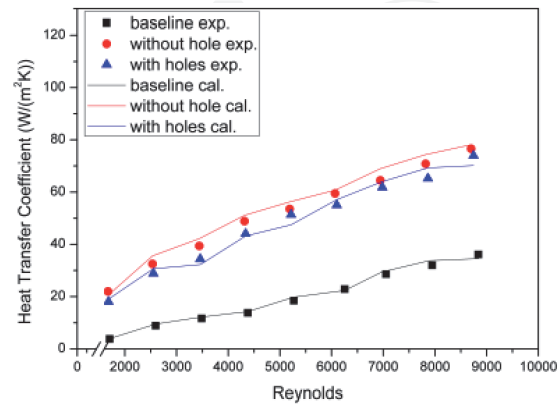


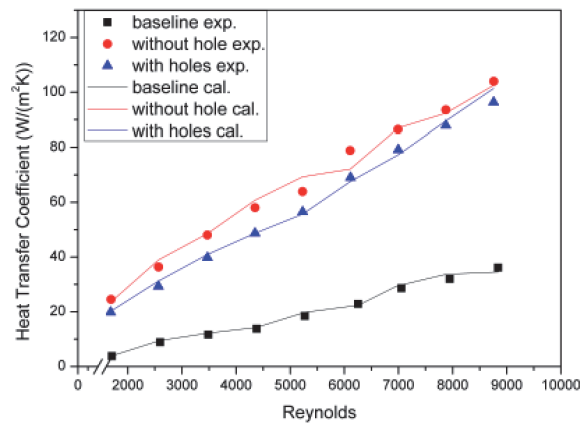
Figure 21.
 Average spanwise Nusselt numbers the RWP and CRWP at a velocity of 2.0 m/s.

Figures 20 and 21 compare the mean spanwise Nusselt numbers in the RWP and CRWP cases at velocities of 0.4 m/s and 2.0 m/s. The use of VG in the channel increases the Nusselt number [30]. **Figures 20 and 21** show that the mean spanwise Nusselt number in the CRWP case is higher than that in the RWP case. This is

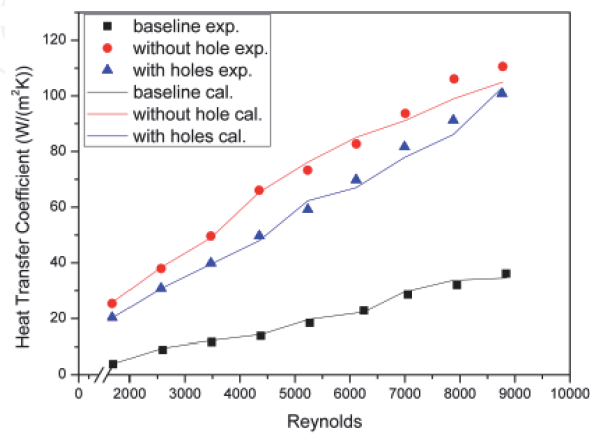
because the longitudinal vortex intensity generated by the CRWP is stronger than that of the RWP. The holes in VG result in a decrease in the mean spanwise Nusselt number because the holes in VG reduce the intensity of the longitudinal vortex [16]. The highest decrease of the average spanwise Nusselt number in perforated RWP and CRWP at a velocity of 0.4 m/s was 24% at $x/L = 0.32$ and 11% at $x/L = 0.56$ of VG without holes, respectively. Whereas for the same case at a velocity of 2.0 m/s, the highest reduction is 2% at $x/L = 0.8$ and 7% at $x/L = 0.32$, respectively.



(a)



(b)

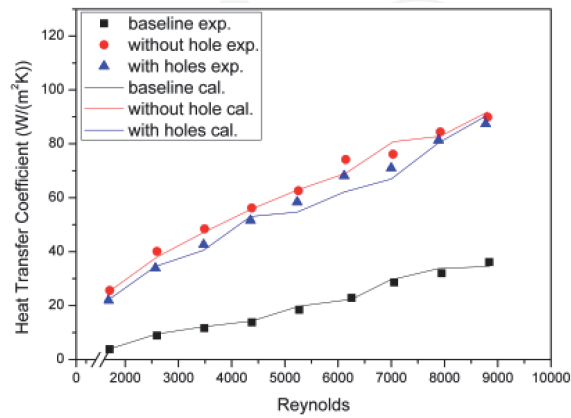


(c)

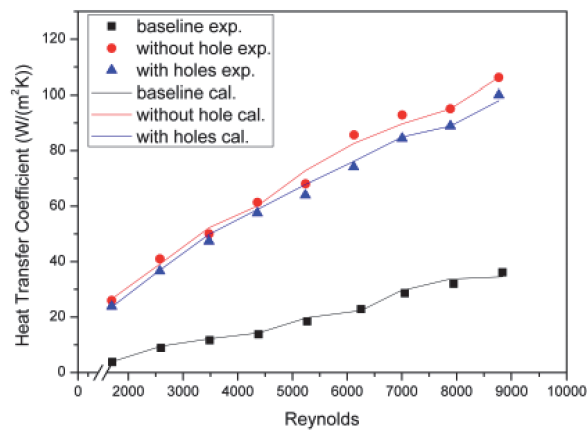
Figure 22. Comparison of the convection heat transfer coefficient on RWP with and without holes for installation: (a) one; (b) two, and (c) three pairs.

3.6 Convection heat transfer coefficient

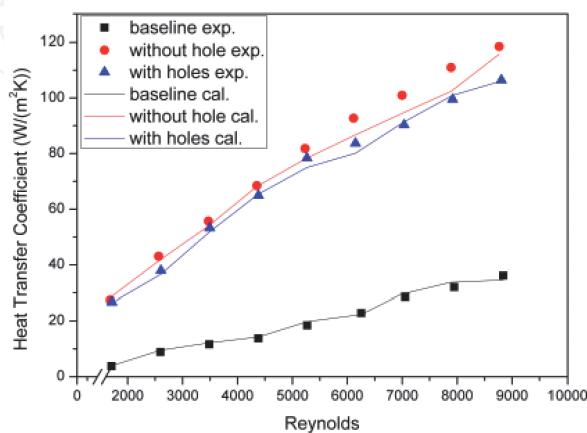
Figures 22 and 23 show the comparison of the heat transfer coefficient values due to the installation of RWP and CRWP. In general, the convection heat transfer coefficient increases with increasing Reynolds number. From Figures 22 and 23, it is found that the convection heat transfer coefficient with the CRWP installation is higher than that of the RWP. This is because CRWP produces a stronger



(a)



(b)

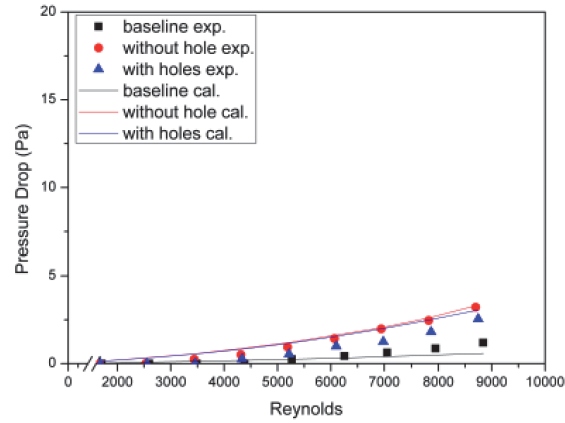


(c)

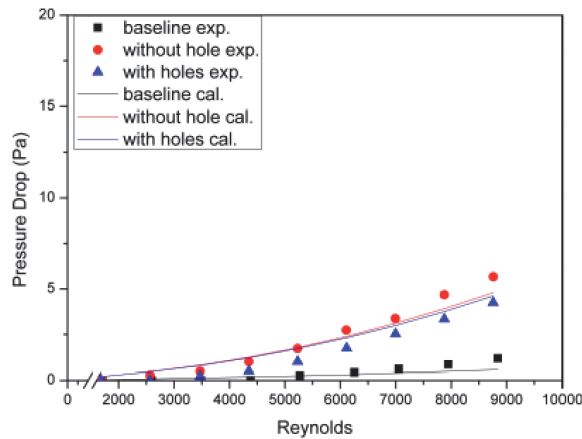
Figure 23. Comparison of the convection heat transfer coefficient on CRWP with and without holes for installation: (a) one; (b) two, and (c) three pairs.

longitudinal vortex intensity than that of RWP due to the instability of the flow as it crosses the CRWP surface [25]. The convection heat transfer coefficient in the RWP and CRWP cases with a three-pair installation configuration with holes is increased by 198% and 207%, respectively, from the baseline at the highest Reynolds number.

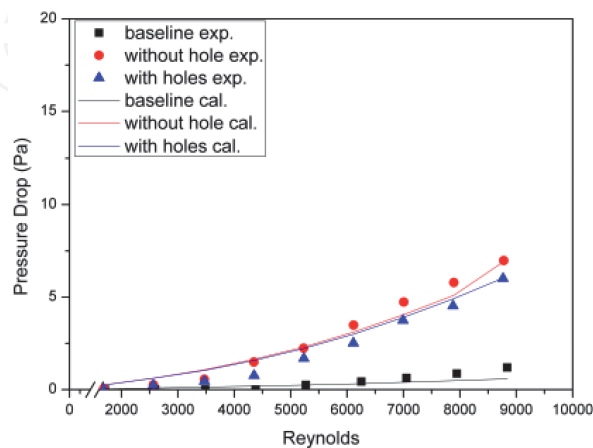
The addition of pairs of VG results in an increase in the convection heat transfer coefficient because the addition of VG pairs strengthens the longitudinal vortex



(a)



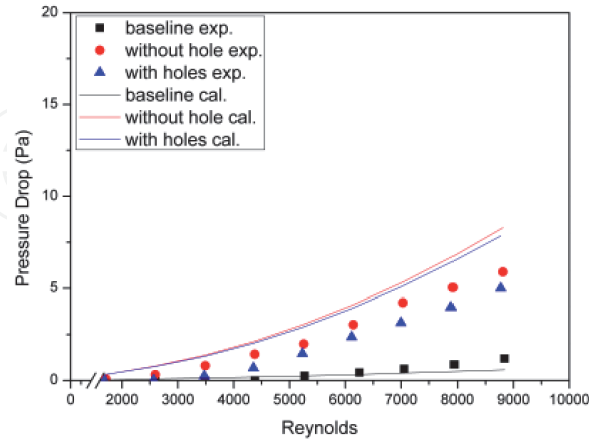
(b)



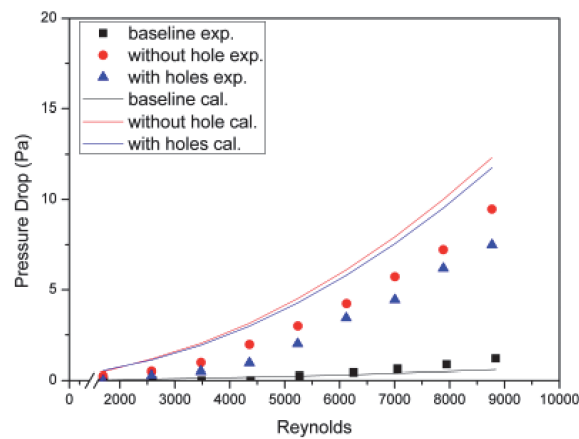
(c)

Figure 24. Comparison of pressure drop on RWP with and without holes for installation: (a) one; (b) two and (c) three pairs.

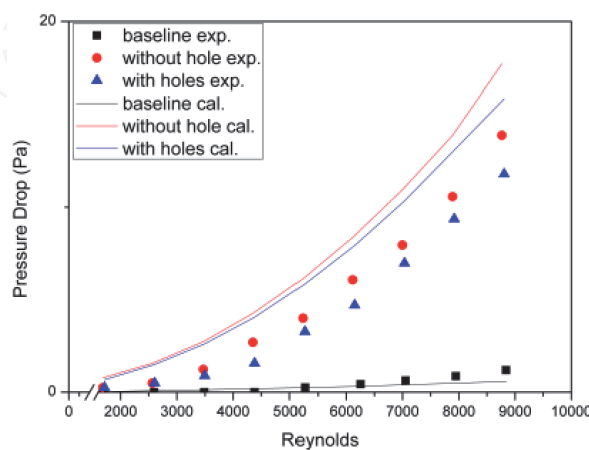
strength and interferes with the formation of boundary layers and increases fluid mixing [29]. Meanwhile, the hole in VG results in a slight decrease in the value of the convection heat transfer coefficient, as seen in **Figures 22 and 23**, because the holes in VG generate jet flow, which can weaken the intensity of the longitudinal vortex [26]. The decrease in the convection heat transfer coefficient at the highest



(a)



(b)



(c)

Figure 25. Comparison of pressure drop on CRWP with and without holes for installation: (a) one; (b) two and (c) three pairs.

Reynolds number for the perforated RWP and CRWP cases of three pairs is 2% and 8% of the without holes, respectively.

3.7 Pressure drop

A comparison of pressure drop between experiment and simulation for the RWP and CRWP cases is observed in **Figures 24** and **25**, respectively. From the two figures, it is found that the pressure drop for all cases increases with increasing Reynolds number. The main reason is the increase in the drag generated with increasing flow velocity [14]. Installation of RWP and CRWP in the channel results in an increase in pressure drop due to the drag formed on the flow. The pressure drop due to CRWP insertion is higher than RWP because CRWP produces a stronger longitudinal vortex than RWP [37]. For the perforated RWP case, the increase in pressure drop with variations of one, two, and three pairs at the highest Reynolds number is 4.26 times, 8.98 times, and 9.96 times, respectively, from the baseline. Meanwhile, for the perforated CRWP case with the highest Reynolds number in the same case, it is 12.52 times, 19.27 times, and 26.31 times from the baseline. The hole in VG causes a decrease in the pressure drop value because the hole in VG reduces fluid resistance due to the longitudinal vortex [31]. The highest reduction in pressure drop due to the hole in the RWP with variations of one, two, and three pairs is 7%, 4%, and 13%, respectively. On the other hand, the decrease in pressure drop on CRWP with the highest Reynolds number for the same case is 5%, 5%, and 11%, respectively.

3.8 Field synergy principle (FSP)

FSP is a method for analyzing improvement in heat transfer rate, which was informed by Guo et al. [38]. In their study, Guo et al. define the increase in the rate of heat transfer by decreasing the angle of the intersection of the velocity vector and the temperature gradient. The energy conservation equation used by Guo et al. in their research are as follows:

$$\rho C_p \int_0^{\delta_t} (U \cdot \nabla T) dy = -\lambda \frac{\partial T}{\partial y} \quad (25)$$

where ρ , C_p , and λ are assumed to be constant so that the dimensionless form of Eq. (25) is

$$\Re_x Pr \int_0^1 (\dot{U} \cdot \dot{\nabla} T) dy = Nu_x \quad (26)$$

where $\dot{U} = U/U_\infty$, $\dot{\nabla} T^* = \frac{\nabla T}{(T_\infty - T_w)/\delta_t}$, $y = y/\delta_t$. U_∞ and T_∞ are the velocity and temperature of the fluid in the free stream region, respectively. Meanwhile, δ_t is the thickness of the thermal boundary layer. Vector dot product, $\dot{U} \cdot \dot{\nabla} T$, in Eq. (26) can be described as follows:

$$\dot{U} \cdot \dot{\nabla} T = |\dot{U}| |\dot{\nabla} T| \cos \beta \quad (27)$$

where β is the angle between the velocity vector and the temperature gradient. Thus, Eq. (27) can be written as follows:

$$\beta = \cos^{-1} \left(\frac{\dot{U} \cdot \dot{\nabla} T}{|\dot{U}| |\dot{\nabla} T|} \right) \quad (28)$$

Figures 26 and **27** illustrate the local synergy angle in the RWP and CRWP cases, respectively, with speeds of 0.4 m/s and 2.0 m/s. In general, inserting VG in the channel reduces the synergy angle because VG generates a longitudinal vortex [39]. The longitudinal vortex alters the flow and temperature fields resulting in improved heat transfer. From **Figures 26** and **27**, it can be observed that the decreased synergy angle is higher in the case of CRWP than that of RWP because the strength of the longitudinal vortex produced by CRWP is stronger than that of

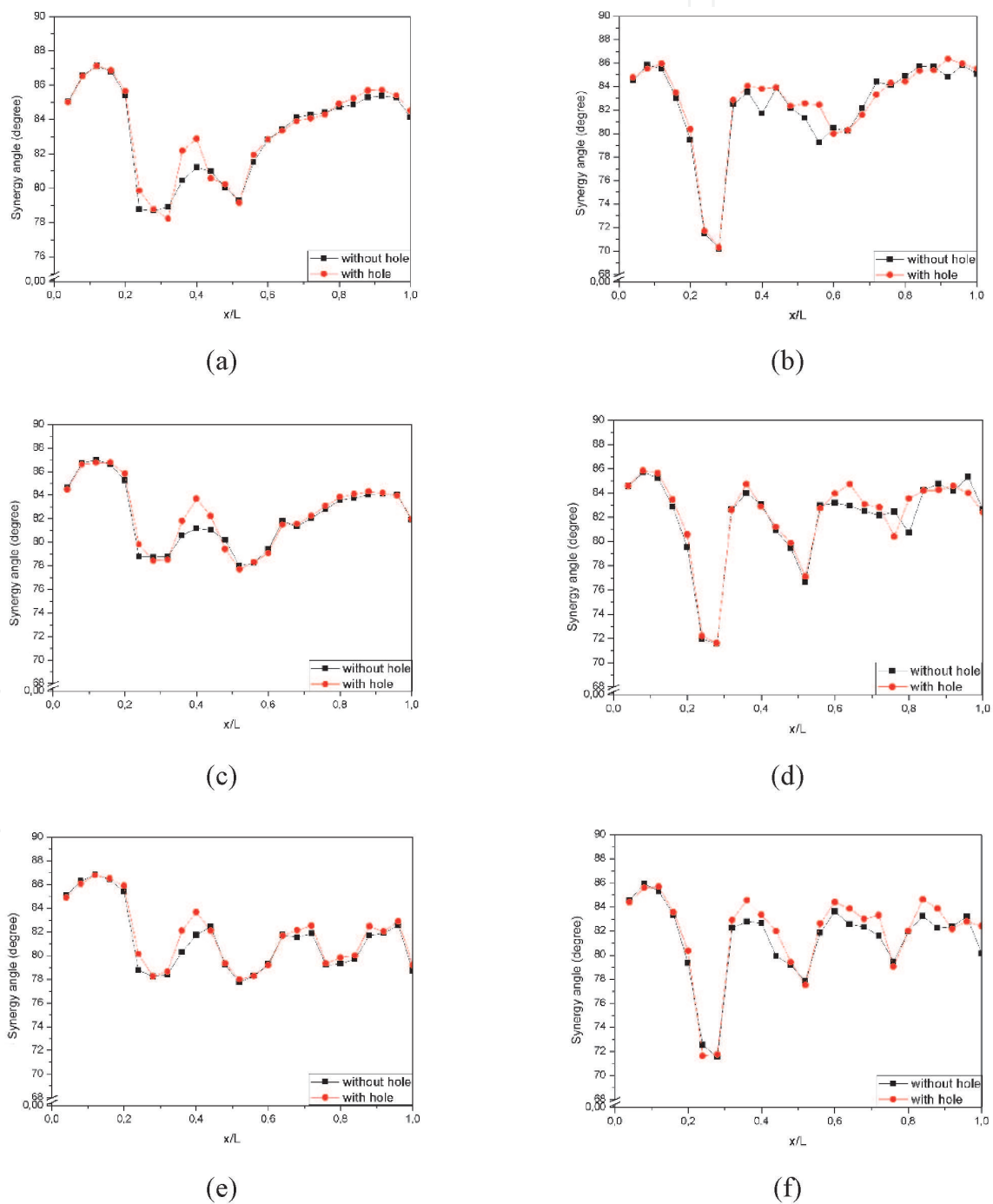


Figure 26. Synergy angle at a speed of 0.4 m/s for the case of (a) one-pair of RWP; (b) one pair of CRWPs; (c) two pairs of RWP; (d) two-pairs of CRWP; (e) three pairs of RWP; (f) three-pairs of CRWP.

RWP [25, 40]. The lowest synergy angle in the case of three pairs of perforated RWP at a velocity of 0.4 m/s are 78.25° , 77.98° , and 79.33° at $x/L = 0.28$, 0.52 , and 0.76 , respectively. Meanwhile, at velocity of 2.0 m/s, they are 81.15° , 79.42° , and 81.19° at $x/L = 0.28$, 0.52 , and 0.76 , respectively.

In the case of CRWP with the same configuration, the largest synergy angles are 71.64° , 77.52° , and 79.04° at $x/L = 0.24$, 0.52 , and 0.76 at 0.4 m/s, respectively. Meanwhile, at velocity of 2.0 m/s, they were 72.68° , 78.81° , and 81.57° at $x/L = 0.28$, 0.52 , and 0.8 , respectively. The hole in VG increases the synergy angle due to a decrease in the heat transfer coefficient [41]. The increase in the mean synergy angle due to the addition of holes in the RWP and CRWP three pairs is 0.25° and 0.29° at a velocity of 2.0 m/s, respectively.

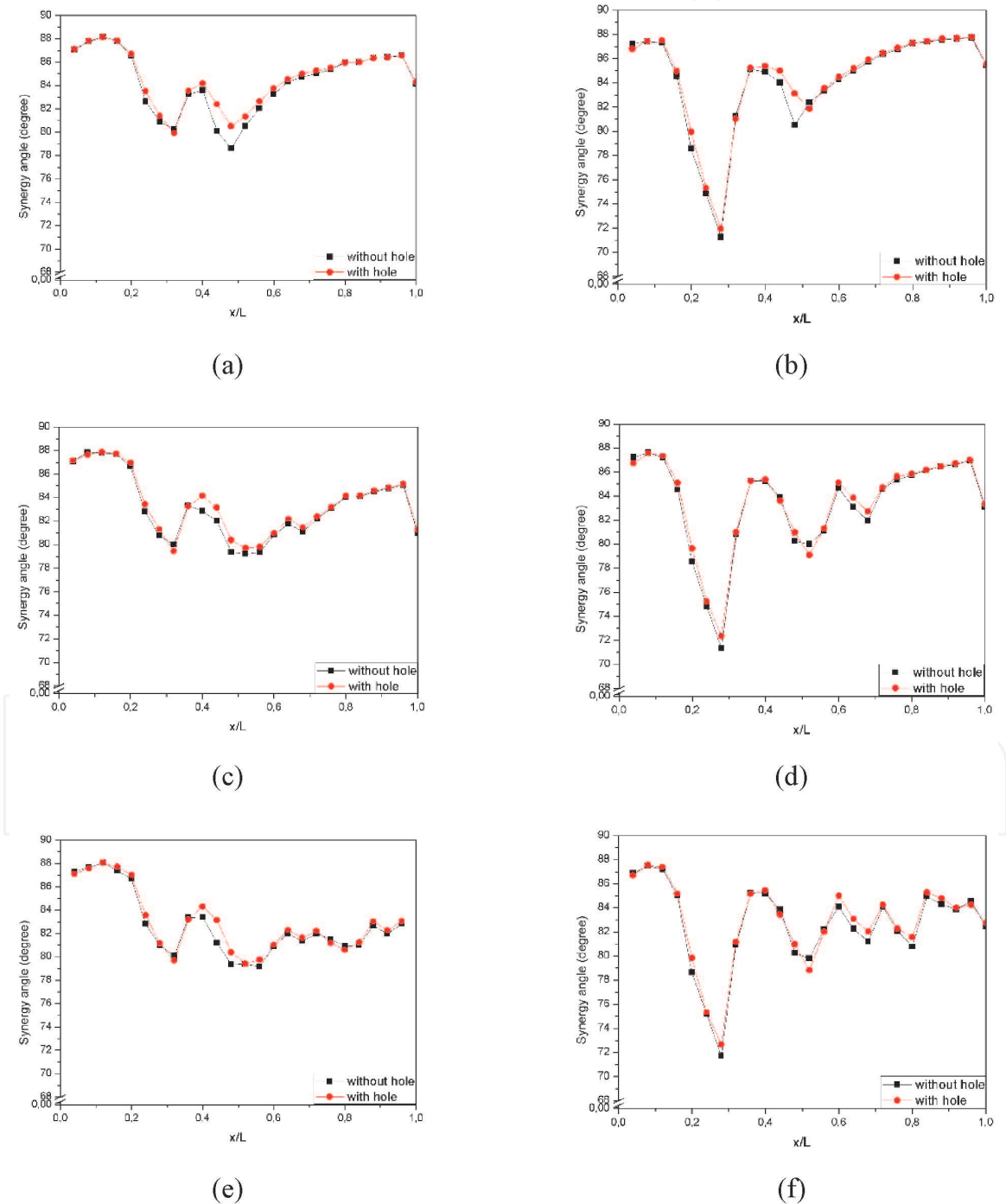


Figure 27. Synergy angle at a speed of 2.0 m/s for the case of (a) one-pair of RWP; (b) one pair of CRWPs; (c) two pairs of RWP; (d) two-pairs of CRWP; (e) three pairs of RWP; (f) three-pairs of CRWP.

4. Conclusion

In this study, a numerical fluid flow simulation was performed to determine the effect of installing RWP and CRWP with/without holes at 45° angle of attack on heat transfer and pressure drop in the rectangular channel. The hole in VG results in a slight decrease in the convection heat transfer coefficient. The reduction of the convection heat transfer coefficient in the channel with the installation of three pairs of perforated RWP and CRWP for the highest Reynolds number was 2% and 8% of the without holes, respectively. The hole in the VG was able to reduce the pressure drop in the channel. The highest reduction in pressure drop due to holes in RWP with variations of one, two, and three pairs was 7%, 4%, and 13%, respectively. On the other hand, the decrease in pressure drop on CRWP with the highest Reynold number for the same case was 5%, 5%, and 11%, respectively. The hole in VG caused a decrease in the mean spanwise Nusselt number in all cases. The decrease in the average spanwise Nusselt number in the perforated RWP and CRWP cases at a velocity of 0.4 m/s was the greatest of 24% at $x/L = 0.32$ and 11% at $x/L = 0.56$, respectively, from those without holes. Whereas for the same case at a velocity of 2.0 m/s, the largest decrease was 2% at $x/L = 0.8$ and 7% at $x/L = 0.32$, respectively. The synergy angle increased due to the holes in the RWP and CRWP. The average synergy angle increase in the use of RWP and CRWP three pairs was 0.25 and 0.29 at a velocity of 2.0 m/s, respectively.

Acknowledgements

This work was supported by the Fundamental Research of Ministry of Education and Culture, Indonesia, with contract number: 225-110/UN7.6.1/PP/2020. The authors are grateful to all research members, especially Lab. Thermofluid of Mechanical Engineering of Diponegoro University, Indonesia.

IntechOpen

Author details

Syaiful* and M. Kurnia Lutfi
Mechanical Engineering Department of Diponegoro University, Semarang,
Indonesia

*Address all correspondence to: syaiful.undip2011@gmail.com

IntechOpen

© 2021 The Author(s). Licensee IntechOpen. This chapter is distributed under the terms of the Creative Commons Attribution License (<http://creativecommons.org/licenses/by/3.0>), which permits unrestricted use, distribution, and reproduction in any medium, provided the original work is properly cited. 

References

- [1] Muhammad Awais, Arafat A. Mint: Heat and mass transfer for compact heat exchanger (CHXs) design: A state-of-the-art review, *International Journal of Heat and Mass Transfer*. 2018; 127; 359–380. DOI: 10.1016/j.ijheatmasstransfer.2018.08.026
- [2] Nares Chimres, Chi-Chuan Wang, Somchai Wongwises. Mint: Effect of elliptical winglet on the air-side performance of fin-and-tube heat exchanger. *International Journal of Heat and Mass Transfer*. 2018; 123; 583–599. DOI: 10.1016/j.ijheatmasstransfer.2018.02.079
- [3] Hui Han, Shaowei Wang, Li Sun, Yuxing Li, Shuo Wang. Mint: Numerical study of thermal and flow characteristics for a fin-and-tube heat exchanger with arc winglet type vortex generators. *International Journal of Refrigeration*. 2018. DOI: 10.1016/j.ijrefrig.2018.10.021
- [4] Pourya Forooghi, Mario Flory, Dirk Bertsche, Thomas Wetzel, Bettina Frohnappfel. Mint: Heat transfer enhancement on the liquid side of an industrially designed flat-tube heat exchanger with passive inserts – Numerical investigation. *Applied Thermal Engineering*. 2017; 123; 573–583. DOI: 10.1016/j.applthermaleng.2017.05.144
- [5] Benjamín Herrmann-Priesnitz, Williams R. Calderón-Muñoz, Gerardo Diaz, Rodrigo Soto. Mint: Heat transfer enhancement strategies in a swirl flow minichannel heat sink based on hydrodynamic receptivity. *International Journal of Heat and Mass Transfer*. 2018; 127; 245–256. DOI: 10.1016/j.ijheatmasstransfer.2018.07.077
- [6] R. Andrzejczyk, T. Muszynski, M. Gosz. Mint: Experimental investigations on heat transfer enhancement in shell coil heat exchanger with variable baffles geometry. *Chemical Engineering & Processing: Process Intensification*. 2018; 132; 114–126. DOI: 10.1016/j.cep.2018.08.017
- [7] Muhammad Awais, Arafat A. Bhuiyan. Mint: Heat transfer enhancement using different types of vortex generators (VGs): A review on experimental and numerical activities. *Thermal Science and Engineering Progress*. 2018; 5; 524–545. DOI: 10.1016/j.tsep.2018.02.007
- [8] H.E. Ahmed, H.A. Mohammed, M.Z. Yusoff. Mint: An overview on heat transfer augmentation using vortex generators and nanofluids: Approaches and applications. *Renewable and Sustainable Energy Reviews*. 2012; 16; 5951–5993. DOI: 10.1016/j.rser.2012.06.003
- [9] Y. Xu, M.D. Islam, N. Kharoua. Mint: Numerical study of winglets vortex generator effects on thermal performance in a circular pipe. *International Journal of Thermal Sciences*. 2017; 112; 304–317. DOI: 10.1016/j.ijthermalsci.2016.10.015
- [10] KeWei Song, Song Liu, LiangBi Wang. Mint: Interaction of counter rotating longitudinal vortices and the effect on fluid flow and heat transfer. *International Journal of Heat and Mass Transfer*. 2016; 93; 349–360. DOI: 10.1016/j.ijheatmasstransfer.2015.10.001
- [11] A. Datta, D. Sanyal, A.K. Das. Mint: Numerical investigation of heat transfer in microchannel using inclined longitudinal vortex generator. *Applied Thermal Engineering*. 2016; 108; 1008–1019. DOI: 10.1016/j.applthermaleng.2016.07.165
- [12] Hung-Yi Li, Wan-Rong Liao, Tian-Yang Li, Yan-Zuo Chang. Mint: Application of vortex generators to heat transfer enhancement of a pin-fin heat

sink. *International Journal of Heat and Mass Transfer*. 2017; 112; 940–949. DOI: 10.1016/j.ijheatmasstransfer.2017.05.032

[13] Hamdi E. Ahmed, M.Z. Yusoff, M. N.A. Hawlader, M.I. Ahmed, B.H. Salman, A.Sh. Kerbeet. Mint: Turbulent heat transfer and nanofluid flow in a triangular duct with vortex generators. *International Journal of Heat and Mass Transfer*. 2017; 105; 495–504. DOI: 10.1016/j.ijheatmasstransfer.2016.10.009

[14] Syaiful, Astrid Ayutasari, Maria F. Soetanto, Ahmad Indra Siswantara, Myung-whan Bae. Mint: Thermo-Hydrodynamics Performance Analysis of Fluid Flow Through Concave Delta Winglet Vortex Generators by Numerical Simulation. *International Journal of Technology*. 2017; 7; 1276–1285. DOI: 10.14716/ijtech.v8i7.706

[15] Mohammad Oneissia, Charbel Habchid, Serge Russeila, Thierry Lemenand, Daniel Bougeard. Mint: Heat transfer enhancement of inclined projected winglet pair vortex generators with protrusions. *International Journal of Thermal Sciences*. 2018; 134; 541–551. DOI:10.1016/j.ijthermalsci.2018.08.032

[16] Zhimin Han, Zhiming Xu, Jingtao Wang. Mint: Numerical simulation on heat transfer characteristics of rectangular vortex generators with a hole. *International Journal of Heat and Mass Transfer*. 2018; 126; 993–1001. DOI: 10.1016/j.ijheatmasstransfer.2018.06.081

[17] M. Samadifar, D. Toghraie. Mint: Numerical simulation of heat transfer enhancement in a plate fin heat exchanger using a new type of vortex generators. *Applied Thermal Engineering*. 2018; 133; 671–681. DOI: 10.1016/j.applthermaleng.2018.01.062

[18] Jiyang Li, Chaobin Dang, Eiji Hihara. Mint: Heat transfer enhancement in a parallel, finless heat exchanger using a longitudinal vortex

generator, Part A: Numerical investigation. *International Journal of Heat and Mass Transfer*. 2019; 128; 87–97. DOI: 10.1016/j.ijheatmasstransfer.2018.06.049

[19] Gaofeng Lu, Xiaoqiang Zhai. Mint: Effects of curved vortex generators on the air-side performance of fin-and tube heat exchangers. *International Journal of Thermal Sciences*. 2019; 136; 509–518. DOI: 10.1016/j.ijthermalsci.2018.11.009

[20] Ralph Kristoffer B. Gallegos, Rajnish N. Sharma. Mint: Heat transfer performance of flag vortex generators in rectangular channels. *International Journal of Thermal Sciences*. 2019; 137; 26–44. DOI: 10.1016/j.ijthermalsci.2018.11.001

[21] L.H. Tang, W.X. Chu, N. Ahmed, M. Zeng. Mint: A New Configuration of Winglet Longitudinal Vortex Generator to Enhance Heat Transfer in a Rectangular Channel. *Applied Thermal Engineering*. 2016; 104; 74–84. DOI: 10.1016/j.applthermaleng.2016.05.056

[22] Syaiful, Arsanti Rakha Siwi, Tony Suryo Utomo, Yurianto, and Retno Wulandari. Mint: Numerical Analysis of Heat and Fluid Flow Characteristics of Airflow Inside Rectangular Channel with Presence of Perforated Concave Delta Winglet Vortex Generators. *International Journal of Heat and Technology*. 2019; 37; 1059–1070. DOI: 10.18280/ijht.370415

[23] ZhaoqingKe, Chung-Lung Chen, Kuojiang Li, Sheng Wang, Chien-Hua Chen. Mint: Vortex dynamics and heat transfer of longitudinal vortex generators in a rectangular channel. *International Journal of Heat and Mass Transfer*. 2019; 132; 871–885. DOI: 10.1016/j.ijheatmasstransfer.2018.12.064

[24] M. Fiebig. Mint: Vortices, Generators and Heat Transfer. *Trans IChemE*. 1998; 76

- [25] Syaiful, Imam Syarifudin, Maria F. Soetanto and Myung-whan Bae. Numerical simulation of heat transfer augmentation in fin-and-tube heat exchanger with various number of rows of concave rectangular winglet vortex generator. In: MATEC Web of Conferences 159; 2018, doi: 10.1051/mateconf/201815902012
- [26] Gaofeng Lu, Guobing Zhou. Mint: Numerical simulation on performances of plane and curved winglet type vortex generator pairs with punched holes. International Journal of Heat and Mass Transfer. 2016; 102; 679–690. DOI: 10.1016/j.ijheatmasstransfer.2016.06.063
- [27] Zhiming Xu, Zhimin Han, Jingtao Wang, Zuodong Liu. Mint: The characteristics of heat transfer and flow resistance in a rectangular channel with vortex generators. International Journal of Heat and Mass Transfer. 2018; 116; 61–72. DOI: 10.1016/j.ijheatmasstransfer.2017.08.083
- [28] Leandro O. Salviano, Daniel J. Dezan, Jurandir I. Yanagihara. Mint: Thermal-hydraulic performance optimization of inline and staggered fin-tube compact heat exchangers applying longitudinal vortex generators. Applied Thermal Engineering. 2015; DOI: 10.1016/j.applthermaleng.2015.11.069.
- [29] Shailesh Kumar Sarangi, Dipti Prasad Mishra. Mint: Effect of winglet location on heat transfer of a fin-and-tube heat exchanger. Applied Thermal Engineering. 2017; 116; 528–540. DOI: 10.1016/j.applthermaleng.2017.01.106
- [30] KeWei Song, Toshio Tagawa, ZhongHao Chena, Qiang Zhang. Mint: Heat transfer characteristics of concave and convex curved vortex generators in the channel of plate heat exchanger under laminar flow. International Journal of Thermal Sciences. 2019; 137; 215–228. DOI: 10.1016/j.ijthermalsci.2018.11.002
- [31] Syaiful, M. S. K. Tony S. U., Agus Saryanto, and Myung-Whan Bae. Improvement of hydrodynamic performance of heated plate mounted by perforated concave delta winglet vortex generator in airflow channel: An experimental study. In: AIP Conference Proceedings 1983, 2018. doi: 10.1063/1.5046200
- [32] Luciano Garelli, Gustavo Ríos Rodríguez, Jonathan J. Dorella, Mario A. Storti. Mint: Heat transfer enhancement in panel type radiators using delta-wing vortex generators. International Journal of Thermal Sciences. 2019; 137; 64–74. DOI: 10.1016/j.ijthermalsci.2018.10.037
- [33] A. Bjerg, K. Christoffersen, H. Sørensen, J. Hærvig. Mint: Flow structures and heat transfer in repeating arrangements of staggered rectangular winglet pairs by Large Eddy Simulations: Effect of winglet height and longitudinal pitch distance. International Journal of Heat and Mass Transfer. 2019; 131; 654–663. DOI: 10.1016/j.ijheatmasstransfer.2018.11.015
- [34] Bittagopal Mondal, Carlos F. Lopez, Ankit Verma, Partha P. Mukherjee. Mint: Vortex generators for active thermal management in lithium-ion battery systems. International Journal of Heat and Mass Transfer. 2018; 124; 800–815. DOI: 10.1016/j.ijheatmasstransfer.2018.04.015
- [35] Muhammad Awais, Arafat A. Bhuiyan. Mint: Enhancement of thermal and hydraulic performance of compact finned-tube heat exchanger using vortex generators (VGs): A parametric study. International Journal of Thermal Sciences. 2019; 140; 154–166. DOI: 10.1016/j.ijthermalsci.2019.02.041
- [36] S.R. Hiravennavar, E.G. Tulapurkara, G. Biswas. Mint: A note on the flow and heat transfer enhancement in a channel with built-in winglet pair. International Journal of Heat and Fluid

Flow. 2007; 28; 299–305. DOI: 10.1016/j.ijheatfluidflow.2006.03.030

[37] Hemant Naik, S. Harikrishnan, Shaligram Tiwari. Mint: Numerical investigations on heat transfer characteristics of curved rectangular winglet placed in a channel. *International Journal of Thermal Sciences*. 2018; 129; 489–503. DOI: 10.1016/j.ijthermalsci.2018.03.028

[38] Z.Y. Guo, D.Y. Li, B.X. Wang. Mint: A novel concept for convective heat transfer enhancement. *International Journal of Heat and Mass Transfer*. 1998; 41; 2221–2225

[39] J.M. Wu, W.Q. Tao. Mint: Numerical study on laminar convection heat transfer in a rectangular channel with longitudinal vortex generator. Part A: Verification of field synergy principle. *International Journal of Heat and Mass Transfer*. 2008; 51; 1179–1191. DOI: 10.1016/j.ijheatmasstransfer.2007.03.032

[40] Gaofeng Lu, Guobing Zhou. Mint: Numerical simulation on performances of plane and curved winglet-Pair vortex generators in a rectangular channel and field synergy analysis. *International Journal of Thermal Sciences*. 2016; 109; 323–333. DOI: 10.1016/j.ijthermalsci.2016.06.024

[41] Z.Y. Guo, W.Q. Tao, R.K. Shah. Mint: The field synergy (coordination) principle and its applications in enhancing single phase convective heat transfer. *International Journal of Heat and Mass Transfer*. 2005; 48; 1797–1807. DOI:10.1016/j.ijheatmasstransfer.2004.11.007